

A Sub-GeV Low Mass Hidden Dark Sector of $SU(2)_H \times U(1)_X$

Raymundo Ramos,^{1,*} Van Que Tran,^{2,†} and Tzu-Chiang Yuan^{1,‡}

¹*Institute of Physics, Academia Sinica, Nangang, Taipei 11529, Taiwan*

²*School of Physics, Nanjing University, Nanjing 210093, China*

(Dated: September 8, 2021)

Abstract

We present a detailed study of the non-abelian vector dark matter candidate W' with a MeV–GeV low mass range, accompanied by a dark photon A' and a dark Z' of similar masses, in the context of a gauged two-Higgs-doublet model with the hidden gauge group that has the same structure as the Standard Model electroweak gauge group. The stability of dark matter is protected by an accidental discrete Z_2 symmetry (h -parity) which was usually imposed *ad hoc* by hand. We examine the model by taking into account various experimental constraints including dark photon searches at NA48, NA64, E141, ν -CAL, BaBar and LHCb experiments, electroweak precision data from LEP, relic density from Planck satellite, direct (indirect) detection of dark matter from CRESST-III, DarkSide-50, XENON1T (Fermi-LAT), and collider physics from the LHC. The theoretical requirements of bounded from below of the scalar potential and tree level perturbative unitarity of the scalar sector are also imposed. The viable parameter space of the model consistent with all the constraints is exhibited. While a dark Z' can be the dominant contribution in the relic density due to resonant annihilation of dark matter, a dark photon is crucial to dark matter direct detection. We also demonstrate that the parameter space can be further probed by various sub-GeV direct dark matter experimental searches at CDEX, NEWS-G and SuperCDMS in the near future.

*Electronic address: raramos@gate.sinica.edu.tw

†Electronic address: vqtran@nju.edu.cn

‡Electronic address: tcyuan@phys.sinica.edu.tw

I. INTRODUCTION

The stability of heavy dark matter (DM) is usually implemented in many particle physics models beyond the standard model (SM) by imposing a discrete Z_2 symmetry in the Lagrangian. These models include the simplest scalar phantom model by adding just a singlet Z_2 -odd scalar field (real or complex) to the SM [1], the popular inert two-Higgs-doublet model (I2HDM) [2, 3], the minimal supergravity standard model with R -parity (MSSM) [4–6], little Higgs model with T -parity (LHM) [7–9] *etc.* In I2HDM, the DM candidate can be either the CP-even or -odd scalar residing in the second Z_2 -odd Higgs doublet. Many detailed analysis of DM phenomenology in the scalar phantom models and I2HDM can be found in the literature in [10–12] and [13–18] respectively. In MSSM, the lightest supersymmetric particle (LSP) for the DM candidate can be the spin 0 sneutrino (the superpartner of neutrino) or the lightest spin 1/2 neutralino [19] (in general a linear combination of two gauginos and two Higgsinos [20]). We note that in some low energy supergravity models, the LSP can be the spin 3/2 gravitino, the superpartner of graviton. For a review of supersymmetric dark matter, see for example [21]. In LHM, the spin 1 T -odd partner of the photon can be the DM candidate whose collider implication was studied in [22]. There are also well-motivated non-abelian dark matter models based on additional gauge group like $SU(2)$ [23–28], in which the extra spin 1 gauge boson W' can be a DM candidate. Moreover, instead of specifying an underlying dark matter model, one can also use the effective dark matter theory approach [29–31] to discuss various dark matter phenomenologies [32–37].

Recently a gauged two-Higgs-doublet model (G2HDM) based on an extended electroweak gauge group $SU(2)_L \times U(1)_Y \times SU(2)_H \times U(1)_X$, was proposed [38], in which a hidden discrete Z_2 symmetry (h -parity) [39] arises naturally as an accidental symmetry rather than imposed by hand. This discrete symmetry ensures the stability of the DM candidate in G2HDM, which can be either a complex scalar (which in general is a linear combination of various fields in the model) or a heavy neutrino ν^H or an extra gauge boson $W'^{(p,m)}$, all of which have odd h -parity. We note that, unlike the left-right symmetric model [40, 41], the $W'^{(p,m)}$ in G2HDM do not carry electric charge.

The novel idea of G2HDM, as compared with many variants of general 2HDM [42], is that the two Higgs doublets H_1 and H_2 of $SU(2)_L$ are grouped into a fundamental representation of a new gauge group $SU(2)_H$. Consistency checks of the model were scrutinized for the

scalar and gauge sectors in [43] and [44] respectively. In [39], a detailed phenomenological analysis of the scalar DM candidate in G2HDM was carried out. In general, the scalar DM candidate is a complex field made up of a linear combination of the components from the inert Higgs doublet H_2 and the $SU(2)_H$ doublet Φ_H and triplet Δ_H . By performing a detailed parameter scan in the model it was demonstrated [39] that only the triplet-like DM is favored when all the constraints from the relic density, direct and indirect searches for the DM are taken into account. As discussed in [38], the triplet Δ_H plays the primary role as a trigger for spontaneous symmetry breaking of the model down to $U(1)_{\text{EM}}$. We note also that this triplet can have topological implications from the hidden sector. Since Δ_H is an adjoint representation of $SU(2)_H$, there exists magnetic monopole [45, 46] and dyon [47] solutions in the hidden sector which may play the role of topological stable DM [48]. However, the triplet is not required to generate realistic mass spectra for all the particles in G2HDM. Therefore if one omits this triplet scalar, the scalar DM candidate is no longer favorable in the parameter space of G2HDM according to the analysis in [39]. However, as mentioned above, there are two other alternative DM candidates in the model. In this paper, we will show that the non-abelian gauge boson $W^{(p,m)}$ associated with $SU(2)_H$ can be a viable DM as well. In particular we will focus on the low mass DM scenario in the MeV–GeV range which has attracted a lot of attention in recent years.

This paper is organized as follows. In Sec. II, we will review some salient features of the simplified G2HDM without introducing the Higgs triplet field Δ_H of the extra $SU(2)_H$. The theoretical constraints on the Higgs potential, electroweak precision data for the Z -boson mass shift from Large Electron-Positron Collider (LEP) data, dark photon constraints from various low energy experiments and the 125 GeV Higgs data constraints from the Large Hadron Collider (LHC) are discussed in Sec. III. We then turn to the experimental constraints of dark matter physics in Sec. IV. The cosmological relic density from Planck satellite [49], underground direct detection constraints from CRESST III [50], DarkSide-50 [51] and XENON1T [52], astrophysical gamma-ray indirect detection constraints from Fermi-LAT [53, 54] and mono-jet constraints from LHC [55–57] for the sub-GeV dark matter $W^{(p,m)}$ in G2HDM are studied in Secs. IV A, IV B, IV C and IV D respectively. Our numerical results are presented in Sec. V. We conclude in Sec. VI. In Appendix A, we discuss the mixing effects in the gauge fixings of the model in a general renormalizable R_ξ gauge. This work can be regarded as an expanded detailed version of the compact and

partial results presented in [58].

II. THE SIMPLIFIED G2HDM MODEL

In this section, we discuss a simplified version of the G2HDM first proposed in [38]. In particular, we will remove the triplet scalar Δ_H in the original model because it is not absolutely required for a realistic particle spectra and the number of free parameters in the scalar potential can be reduced significantly. We note that the Yukawa couplings are not affected by this simplification since the triplet does not couple to the fermions in the model.

A. Particle Content

The gauge group of the simplified G2HDM is the same as in [38],

$$\mathcal{G} = SU(3)_C \times SU(2)_L \times U(1)_Y \times SU(2)_H \times U(1)_X .$$

In Table I, we summarize the matter content and their quantum number assignments in G2HDM. At the minimum risk of confusion, we will continue refer this model as G2HDM to avoid cluttering throughout the paper with the adjective word ‘‘simplified’’. What we are really concerned about is the electroweak part of \mathcal{G} , so the color group $SU(3)_C$ is not relevant in what follows.

B. Higgs Potential and Spontaneous Symmetry Breaking

The most general Higgs potential which is invariant under $SU(2)_L \times U(1)_Y \times SU(2)_H \times U(1)_X$ can be written down as follows

$$\begin{aligned} V = & -\mu_H^2 (H^{\alpha i} H_{\alpha i}) + \lambda_H (H^{\alpha i} H_{\alpha i})^2 + \frac{1}{2} \lambda'_H \epsilon_{\alpha\beta\gamma\delta} (H^{\alpha i} H_{\gamma i}) (H^{\beta j} H_{\delta j}) \\ & -\mu_\Phi^2 \Phi_H^\dagger \Phi_H + \lambda_\Phi (\Phi_H^\dagger \Phi_H)^2 + \lambda_{H\Phi} (H^\dagger H) (\Phi_H^\dagger \Phi_H) + \lambda'_{H\Phi} (H^\dagger \Phi_H) (\Phi_H^\dagger H), \end{aligned} \quad (1)$$

where $(\alpha, \beta, \gamma, \delta)$ and (i, j) refer to the $SU(2)_H$ and $SU(2)_L$ indices respectively, all of which run from 1 to 2, and $H^{\alpha i} = H_{\alpha i}^*$.

To facilitate spontaneous symmetry breaking (SSB) and obtain the particle mass spectra

Matter Fields	$SU(3)_C$	$SU(2)_L$	$SU(2)_H$	$U(1)_Y$	$U(1)_X$	h -parity
$Q_L = (u_L \ d_L)^T$	3	2	1	1/6	0	++
$U_R = (u_R \ u_R^H)^T$	3	1	2	2/3	1	+ -
$D_R = (d_R^H \ d_R)^T$	3	1	2	-1/3	-1	- +
u_L^H	3	1	1	2/3	0	-
d_L^H	3	1	1	-1/3	0	-
$L_L = (\nu_L \ e_L)^T$	1	2	1	-1/2	0	++
$N_R = (\nu_R \ \nu_R^H)^T$	1	1	2	0	1	+ -
$E_R = (e_R^H \ e_R)^T$	1	1	2	-1	-1	- +
ν_L^H	1	1	1	0	0	-
e_L^H	1	1	1	-1	0	-
$H = (H_1 \ H_2)^T$	1	2	2	1/2	1	+ -
$\Phi_H = (\Phi_1 \ \Phi_2)^T$	1	1	2	0	1	- +
\mathcal{S}	1	1	1	0	0	+

TABLE I: Matter content and their quantum number assignments in G2HDM. The electric charge Q in unit of positron charge e is given by $Q = T_L^3 + Y$. The scalar \mathcal{S} in the last row is the Stueckelberg field introduced in [38] to give mass for the $U(1)_X$ gauge boson.

of the model, we shift the fields based on our conventional wisdom

$$H_1 \equiv \begin{pmatrix} H_{11} \\ H_{12} \end{pmatrix} = \begin{pmatrix} G^+ \\ \frac{v+h}{\sqrt{2}} + i\frac{G^0}{\sqrt{2}} \end{pmatrix}, \quad H_2 \equiv \begin{pmatrix} H_{21} \\ H_{22} \end{pmatrix} = \begin{pmatrix} H^+ \\ H_2^0 \end{pmatrix}, \quad \Phi_H = \begin{pmatrix} G_H^p \\ \frac{v_\Phi+\phi_2}{\sqrt{2}} + i\frac{G_H^0}{\sqrt{2}} \end{pmatrix}, \quad (2)$$

where v and v_Φ are the vacuum expectation values (VEV) of H_1 and Φ_H fields respectively. H_2 is the inert doublet in G2HDM and hence does not have VEV. Naively we would think that the Goldstone bosons G^+ , G_H^p , G^0 and G_H^0 will be absorbed by the longitudinal components of W^+ , W'^p , W^3 and W'^3 respectively. In Appendix A we will show that the last three Goldstone fields have mixing effects with other fields in the scalar sector that makes the situation more interesting but a little bit more complicated.

Substituting the scalar field decomposition of Eq. (2) into the scalar potential Eq. (1)

and then minimize the potential, one can obtain the solutions of VEVs as follows

$$v^2 = \frac{2(\lambda_{H\Phi}\mu_\Phi^2 - 2\lambda_\Phi\mu_H^2)}{\lambda_{H\Phi}^2 - 4\lambda_H\lambda_\Phi}, \quad (3)$$

$$v_\Phi^2 = \frac{2(\lambda_{H\Phi}\mu_H^2 - 2\lambda_H\mu_\Phi^2)}{\lambda_{H\Phi}^2 - 4\lambda_H\lambda_\Phi}. \quad (4)$$

Equivalently, we can use the minimization conditions to trade μ_H^2 and μ_Φ^2 with v and v_Φ as

$$\mu_H^2 = \lambda_H v^2 + \frac{\lambda_{H\Phi} v v_\Phi^2}{2}, \quad (5)$$

$$\mu_\Phi^2 = \lambda_\Phi v_\Phi^2 + \frac{\lambda_{H\Phi} v^2}{2}. \quad (6)$$

C. Scalar Mass Spectrum

In the $S = \{h, \phi_2\}$ basis the mass matrix is given as

$$\mathcal{M}_S^2 = \begin{pmatrix} 2\lambda_H v^2 & \lambda_{H\Phi} v v_\Phi \\ \lambda_{H\Phi} v v_\Phi & 2\lambda_\Phi v_\Phi^2 \end{pmatrix}. \quad (7)$$

One can use an orthogonal transformation O^S , which can be parametrized as

$$O^S = \begin{pmatrix} \cos \theta_1 & \sin \theta_1 \\ -\sin \theta_1 & \cos \theta_1 \end{pmatrix}, \quad (8)$$

where

$$\tan 2\theta_1 = \frac{2\mathcal{M}_{S12}^2}{\mathcal{M}_{S22}^2 - \mathcal{M}_{S11}^2} = \frac{\lambda_{H\Phi} v v_\Phi}{\lambda_\Phi v_\Phi^2 - \lambda_H v^2}, \quad (9)$$

to diagonalize \mathcal{M}_S^2 ,

$$(O^S)^T \cdot \mathcal{M}_S^2 \cdot O^S = \text{Diag}(m_{h_1}^2, m_{h_2}^2), \quad (10)$$

with h_1 being identified as the 125 GeV SM-like Higgs boson and h_2 as a heavier scalar boson. The mass squared eigenvalues of Eq. (7) are given by

$$m_{h_{1,2}}^2 = \lambda_H v^2 + \lambda_\Phi v_\Phi^2 \mp \sqrt{\lambda_H^2 v^4 - 2\lambda_H \lambda_\Phi v^2 v_\Phi^2 + \lambda_{H\Phi}^2 v^2 v_\Phi^2 + \lambda_\Phi^2 v_\Phi^4}. \quad (11)$$

In the basis of $S' = \{G_H^p, H_2^{0*}\}$, we obtain the mass matrix:

$$\mathcal{M}_{S'}^2 = \frac{1}{2} \lambda'_{H\Phi} \begin{pmatrix} v^2 & v v_\Phi \\ v v_\Phi & v_\Phi^2 \end{pmatrix}. \quad (12)$$

Similarly, this mass matrix can be diagonalized by an orthogonal matrix,

$$O^{S'} = \begin{pmatrix} \cos \theta_2 & \sin \theta_2 \\ -\sin \theta_2 & \cos \theta_2 \end{pmatrix}, \quad (13)$$

where

$$\tan 2\theta_2 = \frac{2\mathcal{M}_{S'12}^2}{\mathcal{M}_{S'22}^2 - \mathcal{M}_{S'11}^2} = \frac{2vv_\Phi}{v_\Phi^2 - v^2}, \quad (14)$$

which gives

$$\left(O^{S'}\right)^T \cdot \mathcal{M}_{S'}^2 \cdot O^{S'} = \text{Diag} (0, m_D^2). \quad (15)$$

We note that, in Eq. (15), the zero eigenvalue corresponds to the Nambu-Goldstone boson mass eigenstate \tilde{G}_H^p , while the other eigenvalue

$$m_D^2 = \frac{1}{2}\lambda'_{H\Phi}(v^2 + v_\Phi^2), \quad (16)$$

is the mass of a new dark scalar boson.

The charged Higgs boson mass is given as

$$m_{H^\pm}^2 = \frac{1}{2}(\lambda'_{H\Phi}v_\Phi^2 - \lambda'_H v^2). \quad (17)$$

The Goldstone bosons G^0 and G_H^0 are massless.

The above scalar mass spectrum is derived in the so-called 't Hooft-Landau gauge. We will discuss further the mixing effects of the Goldstone bosons with other scalar fields in a general renormalizable R_ξ gauge in Appendix A.

We note that $h_{1,2}$, G^0 and G_H^0 are even under h -parity, while \tilde{G}_H^p , D and H^\pm are odd [39].

D. Gauge Sector

After SSB, the W^\pm gauge boson of $SU(2)_L$ remains the same as in SM with its mass given by $m_W = gv/2$. The $SU(2)_H$ gauge boson $W'^{(p,m)}$ receives mass from $\langle H_1 \rangle$ and $\langle \Phi_2 \rangle$ given by

$$m_{W'} = \frac{1}{2}g_H\sqrt{v^2 + v_\Phi^2}. \quad (18)$$

Note that $W'^{(p,m)}$ are electrically neutral and thus do not mix with the SM W^\pm . In addition, $W'^{(p,m)}$ is odd under h -parity. If it is the lightest h -parity odd particle in the model, it will be stable and can be a DM candidate.

On the other hand, the SM neutral gauge bosons B and W^3 can mix with the new gauge bosons W'^3 and X , all of which have even h -parity. Together with the Stueckelberg mass parameters M_X and M_Y for the two abelian groups $U(1)_X$ and $U(1)_Y$, SSB generates a 4×4 neutral gauge boson mass matrix in the basis of $\{B, W^3, W'^3, X\}$ [38, 44]. Due to the theoretical motivations or prejudices mentioned in Ref. [44], we set the Stueckelberg mass $M_Y = 0$. Applying the weak rotation on upper left 2×2 block of the 4×4 mass matrix, one obtains immediately a zero eigenvalue identified as the SM photon and a 3×3 sub-matrix in the basis of $\{Z^{\text{SM}}, W'^3, X\}$ given by [44],

$$\mathcal{M}_Z^2 = \begin{pmatrix} m_{Z^{\text{SM}}}^2 & -\frac{g_H v}{2} m_{Z^{\text{SM}}} & -g_X v m_{Z^{\text{SM}}} \\ -\frac{g_H v}{2} m_{Z^{\text{SM}}} & m_{W'}^2 & \frac{g_X g_H (v^2 - v_\Phi^2)}{2} \\ -g_X v m_{Z^{\text{SM}}} & \frac{g_X g_H (v^2 - v_\Phi^2)}{2} & g_X^2 (v^2 + v_\Phi^2) + M_X^2 \end{pmatrix}, \quad (19)$$

where g , g' , g_H and g_X are the gauge couplings of $SU(2)_L$, $U(1)_Y$, $SU(2)_H$ and $U(1)_X$ respectively, and $m_{Z^{\text{SM}}} = v\sqrt{g^2 + g'^2}/2$ is the SM Z boson mass expression. The mass matrix in Eq. (19) can be diagonalized by an orthogonal rotation matrix \mathcal{O} so that ¹

$$\begin{pmatrix} Z^{\text{SM}} \\ W'^3 \\ X \end{pmatrix} = \mathcal{O} \cdot \begin{pmatrix} Z \\ Z' \\ A' \end{pmatrix}. \quad (20)$$

In this analysis, we arrange the neutral gauge boson masses as $m_{A'} < m_{Z'} < m_Z \simeq m_{Z^{\text{SM}}}$ with Z identified as the physical Z boson with mass 91.1876 ± 0.0021 GeV [59]—the first heavy neutral vector gauge boson discovered in 1983 at the Super Proton Synchrotron at CERN. Two more massive neutral vector gauge bosons are predicted in G2HDM.

By means of a few assumptions motivated by our expectations, it is possible to draw a few conclusions from Eq. (19). First, the new gauge couplings g_H and g_X are expected to be much smaller than the SM g and g' to avoid large effects on the very precise measurements of the Z properties. Second, the scale of v_Φ is expected to be larger than v given that it characterizes the scale of new physics and is directly related to the masses of beyond the SM (BSM) states. By neglecting any term composed by a product of any three or more of g_H , g_X and v^2/v_Φ^2 it is possible to put Eq. (19) into a block diagonal matrix where only W'^3

¹ The analytical expression of this rotation matrix can be found in Ref. [44].

and X mix resulting in the approximation

$$m_Z \approx m_{Z^{\text{SM}}} . \quad (21)$$

Moreover, the 2×2 squared mass matrix of W'^3 and X can be easily diagonalized and somewhat simple approximations can be found. Since we want the hierarchy $m_{A'} < m_{Z'} < m_{Z^{\text{SM}}}$, the M_X parameter is required to have a value smaller than v . Assuming $M_X < v$ allows us to expand the squared root in the general solution for the eigenvalues of a 2×2 matrix resulting in the following approximations

$$m_{Z'}^2 \approx m_{W'}^2 \left(1 + \frac{4g_X^2}{g_H^2} \right) + M_X^2 \left[1 - \left(1 + \frac{4g_X^2}{g_H^2} + \frac{M_X^2}{m_{W'}^2} \right)^{-1} \right] , \quad (22)$$

$$m_{A'}^2 \approx M_X^2 \left(1 + \frac{4g_X^2}{g_H^2} + \frac{M_X^2}{m_{W'}^2} \right)^{-1} , \quad (23)$$

where $m_{W'}^2 \approx g_H^2 v_\Phi^2 / 4$ was used. From these expressions we can see that $m_{Z'} \gtrsim m_{W'}$ and $m_{A'} \lesssim M_X$.

Since the couplings of the extra gauge bosons, Z' and A' , to the SM fermions are proportional to the new gauge couplings g_H and/or g_X which are in general much smaller than the SM couplings g and g' , the Drell-Yan type processes are suppressed and this can explain the null results of BSM neutral gauge bosons searches at LEP.

In our study, the couplings of the extra gauge bosons to the SM charged leptons and to quarks u and d will be important for dark photon constraints and direct detection of DM. The vectorial and axial parts of their couplings are given by

$$v_\ell^{Z^{(i)}} = \mathcal{O}_{1i} \left(-\frac{1}{2} + 2s_W^2 \right) - \frac{1}{\sqrt{g^2 + g'^2}} \left(g_X \mathcal{O}_{3i} + \frac{1}{2} g_H \mathcal{O}_{2i} \right) , \quad (24)$$

$$v_u^{Z^{(i)}} = \mathcal{O}_{1i} \left(\frac{1}{2} - \frac{4}{3} s_W^2 \right) + \frac{1}{\sqrt{g^2 + g'^2}} \left(g_X \mathcal{O}_{3i} + \frac{1}{2} g_H \mathcal{O}_{2i} \right) , \quad (25)$$

$$v_d^{Z^{(i)}} = \mathcal{O}_{1i} \left(-\frac{1}{2} + \frac{2}{3} s_W^2 \right) - \frac{1}{\sqrt{g^2 + g'^2}} \left(g_X \mathcal{O}_{3i} + \frac{1}{2} g_H \mathcal{O}_{2i} \right) , \quad (26)$$

$$a_\ell^{Z^{(i)}} = -a_u^{Z^{(i)}} = a_d^{Z^{(i)}} = -\frac{\mathcal{O}_{1i}}{2} + \frac{1}{\sqrt{g^2 + g'^2}} \left(g_X \mathcal{O}_{3i} + \frac{1}{2} g_H \mathcal{O}_{2i} \right) , \quad (27)$$

where $i = 1, 2, 3$ and $Z(1) \equiv Z$, $Z(2) \equiv Z'$, $Z(3) \equiv A'$. Using the relations between mixing matrix elements and mixing angles in Eqs. (2.6) to (2.9) of Ref. [44], we can find the following relation

$$\frac{2}{\sqrt{g^2 + g'^2}} \frac{(g_X \mathcal{O}_{3i} + \frac{1}{2} g_H \mathcal{O}_{2i})}{\mathcal{O}_{1i}} = 1 - \frac{m_{Z^{(i)}}^2}{m_{Z^{\text{SM}}}^2} , \quad (28)$$

which can be used to simplify the above vectorial and axial couplings to obtain

$$v_\ell^{Z(i)} = -\mathcal{O}_{1i} \left(1 - 2s_W^2 - \frac{r_i^2}{2} \right), \quad (29)$$

$$v_u^{Z(i)} = \mathcal{O}_{1i} \left(1 - \frac{4}{3}s_W^2 - \frac{r_i^2}{2} \right), \quad (30)$$

$$v_d^{Z(i)} = -\mathcal{O}_{1i} \left(1 - \frac{2}{3}s_W^2 - \frac{r_i^2}{2} \right), \quad (31)$$

$$a_\ell^{Z(i)} = -a_u^{Z(i)} = a_d^{Z(i)} = -\frac{\mathcal{O}_{1i}}{2} r_i^2, \quad (32)$$

where $r_i = m_{Z(i)}/m_{Z^{\text{SM}}}$. In this form, it is obvious that the axial couplings magnitude is expected to be smaller than the ratio of squared masses r_i^2 , which, *e.g.*, for $m_{Z(i)} = 1$ GeV is already close to 10^{-4} . In contrast, the vectorial couplings have an r_i -independent part whose size is controlled by the mixing matrix element \mathcal{O}_{1i} that also affects axial couplings. Therefore, for sufficiently light Z' and A' , the contributions from the axial couplings are expected to be subleading.

The neutral current interactions induced by $W'^{(p,m)}$ are given by

$$\mathcal{L}(W') = g_H (J^{p\mu} W'_\mu + \text{H.c.}), \quad (33)$$

where

$$J^{p\mu} = \frac{1}{\sqrt{2}} \left[\overline{u}_R V_u^H \gamma^\mu u_R^H + \overline{d}_R^H (V_d^H)^\dagger \gamma^\mu d_R + \overline{\nu}_R V_\nu^H \gamma^\mu \nu_R^H + \overline{e}_R^H (V_e^H)^\dagger \gamma^\mu e_R \right], \quad (34)$$

with V_u^H , V_d^H , V_ν^H and V_e^H being the new unitary mass rotation matrices for the fermions. The neutral current interactions induced by Z , Z' , A' bosons can be found in Ref. [44].

E. Free Parameters

From the scalar potential we recognize 9 free parameters including couplings and VEVs. Of those 9 parameters, μ_H^2 and μ_Φ^2 can be related to other parameters using the minimization conditions according to Eqs. (5) and (6), leaving only 7 free parameters. Furthermore, Eq. (10) can be used to relate the parameters λ_H , λ_Φ and $\lambda_{H\Phi}$ to the physical squared

masses $m_{h_1}^2$, $m_{h_2}^2$ and the mixing angle θ_1 obtaining the following relations

$$\lambda_H = \frac{1}{2v^2} (m_{h_1}^2 \cos^2 \theta_1 + m_{h_2}^2 \sin^2 \theta_1) , \quad (35)$$

$$\lambda_\Phi = \frac{1}{2v_\Phi^2} (m_{h_1}^2 \sin^2 \theta_1 + m_{h_2}^2 \cos^2 \theta_1) , \quad (36)$$

$$\lambda_{H\Phi} = \frac{1}{2vv_\Phi} [(m_{h_2}^2 - m_{h_1}^2) \sin(2\theta_1)] . \quad (37)$$

Using the mass of D , Eq. (16), we can express $\lambda'_{H\Phi}$ in the form

$$\lambda'_{H\Phi} = \frac{2m_D^2}{v^2 + v_\Phi^2} . \quad (38)$$

Using this last expression and the mass of the charged Higgs of Eq. (17), we can write λ'_H as

$$\lambda'_H = \frac{2}{v^2} \left[\frac{m_D^2 v_\Phi^2}{v^2 + v_\Phi^2} - m_{H^\pm}^2 \right] . \quad (39)$$

Finally, we can use Eq. (18) to relate v_Φ to the W' mass as

$$v_\Phi^2 = \frac{4m_{W'}^2}{g_H^2} - v^2 . \quad (40)$$

Using the expressions in this subsection allow us to trade six model parameters with five physical squared masses and one mixing angle,

$$\lambda_H, \lambda_\Phi, \lambda_{H\Phi}, \lambda'_{H\Phi}, \lambda'_H, v_\Phi \quad \rightarrow \quad m_{h_1}^2, m_{h_2}^2, m_D^2, m_{H^\pm}^2, m_{W'}^2, \theta_1 . \quad (41)$$

The remaining free parameters of the model are the heavy fermion masses m_{f_H} , the Stueckelberg mass M_X , and the gauge couplings g_X and g_H . Considering that the mass of the Higgs, m_{h_1} , has already been measured [59], we are left with a total of 8 free parameters plus the masses for 12 heavy hidden fermions. The effects of heavy hidden fermions in complex scalar dark matter phenomenology in G2HDM was analyzed in [60].

III. CONSTRAINTS

In this section, we examine the model using various constraints including the theoretical constraints of the scalar potential, electroweak precision data, dark photon physics and Higgs measurements at LHC. DM constraints are presented separately in the next section.

A. Theoretical Constraints

The theoretical constraints on the original G2HDM were studied in Ref. [43]. Here, we follow closely on the steps of that work but remove the scalar triplet and related parameters from the original model.

Vacuum Stability: To make sure the scalar potential is bounded from below, the sum of all quartic terms in the scalar potential needs to be positive. In the same way as Ref. [43] we use copositivity conditions given by the following constraints

$$\tilde{\lambda}_H(\eta) \geq 0, \quad \lambda_\Phi \geq 0, \quad \tilde{\lambda}_{H\Phi}(\xi) + 2\sqrt{\tilde{\lambda}_H(\eta)\lambda_\Phi} \geq 0, \quad (42)$$

where $\tilde{\lambda}_H(\eta) \equiv \lambda_H + \eta\lambda'_H$ and $\tilde{\lambda}_{H\Phi}(\xi) \equiv \lambda_{H\Phi} + \xi\lambda'_{H\Phi}$. The conditions of Eq. (42) have to be met for any value of ξ and η in the ranges $0 \leq \xi \leq 1$ and $-1 \leq \eta \leq 0$.

Perturbative Unitarity: It is required that the parameter space remains within the perturbative limits. To this end, here we compute the $2 \rightarrow 2$ scalar scattering amplitudes induced by the quartic couplings. The $2 \rightarrow 2$ processes induced by vertices from scalar cubic couplings and gauge interactions are suppressed by large momentum exchange in their propagators [43].

Perturbative unitarity requires

$$|\lambda_H|, |\lambda_\Phi| \leq 4\pi, \quad |\lambda_{H\Phi}| \leq 8\pi, \quad |\lambda'_{H\Phi}|, |\lambda'_H| \leq 8\sqrt{2}\pi, \quad (43)$$

$$|2\lambda_H \pm \lambda'_H| \leq 8\pi, \quad |\lambda_{H\Phi} + \lambda'_{H\Phi}| \leq 8\pi, \quad (44)$$

$$\left| (\lambda_H + \lambda'_H/2 + \lambda_\Phi) \pm \sqrt{2\lambda_{H\Phi}^2 + (\lambda_H + \lambda'_H/2 - \lambda_\Phi)^2} \right| \leq 8\pi, \quad (45)$$

$$\left| (5\lambda_H - \lambda'_H/2 + 3\lambda_\Phi) \pm \sqrt{(5\lambda_H - \lambda'_H/2 - 3\lambda_\Phi)^2 + 2(2\lambda_{H\Phi} + \lambda'_{H\Phi})^2} \right| \leq 8\pi. \quad (46)$$

B. Electroweak Constraints

A comprehensive study on the electroweak precision constraints in the original model has been preformed in Ref. [44]. We found that the Z mass shift is the most stringent among all the electroweak precision constraints. In particular, for the parameter space of interest in our analysis, *i.e.*, $g_H \sim g_X \ll 1$ and $(m_{W'}^2, M_X^2) \ll m_{Z\text{SM}}^2$, the Z mass shift, $|\Delta m_Z| = |m_Z - m_{Z\text{SM}}|$, can be estimated as follows

$$\left| \frac{\Delta m_Z}{m_{Z\text{SM}}} \right| \simeq \frac{5g_H^2}{2g_Z^2} \left(1 + \frac{7m_{W'}^2}{5m_{Z\text{SM}}^2} - \frac{4M_X^2}{5m_{Z\text{SM}}^2} \right)^{-1}, \quad (47)$$

where $g_Z = g/\cos\theta_W$ with θ_W being the Weinberg angle. Following the methodology of Ref. [61], we can obtain the experimental uncertainty of the Z mass as

$$\left[\frac{\delta m_Z}{m_{Z\text{SM}}}\right]^2 = \left[\frac{c_W^{-2} - 2t_W^2}{\delta m_W^{-1} m_W}\right]^2 + \frac{t_W^4 (\delta\Delta r)^2}{4(1 - \Delta r)^2}, \quad (48)$$

where $t_W = \tan\theta_W$ and Δr is the radiative correction. Using the PDG values [59] of $m_W \pm \delta m_W = 80.387 \pm 0.016$ GeV, $\Delta r \pm \delta\Delta r = 0.03652 \mp 0.00021 \pm 0.00007$ and $\sin\theta_W = 0.22343$, and by requiring $|\Delta m_Z| < |\delta m_Z|$, one obtains an upper bound on g_H and g_X

$$|g_X| \sim |g_H| \lesssim 0.006 \times \sqrt{1 - \frac{7}{5} \frac{m_{W'}^2}{m_{Z\text{SM}}^2} + \frac{4}{5} \frac{M_X^2}{m_{Z\text{SM}}^2}}. \quad (49)$$

C. Dark Photon

The light boson A' can be treated as a dark photon and, therefore, dark photon constraints have to be applied. In particular, due to the vertex $A'\bar{\ell}\ell$, where ℓ represents any charged lepton, it is expected that for a sufficiently large coupling it should be possible to observe the A' resonance in the invariant mass distribution of e^+e^- and $\mu^+\mu^-$. Dark photon experiments constrain the size of the coupling via a parameter ε_ℓ . In the decay width $\Gamma(A' \rightarrow \ell\bar{\ell})$ the parameter ε_ℓ appears as [62]

$$\Gamma(A' \rightarrow \bar{\ell}\ell) = \frac{\alpha}{3} \varepsilon_\ell^2 m_{A'} \sqrt{1 - \mu_\ell^2} \left(1 + \frac{\mu_\ell^2}{2}\right), \quad (50)$$

where $\mu_\ell = 2m_\ell/m_{A'} < 1$ since this decay channel only opens for $m_{A'} > 2m_\ell$. In the G2HDM, the parameter ε_ℓ at tree level is given by

$$\varepsilon_\ell = \frac{1}{2s_W c_W} \sqrt{(v_\ell^{A'})^2 + (a_\ell^{A'})^2 \left(\frac{1 - \mu_\ell^2}{1 + \mu_\ell^2/2}\right)}, \quad (51)$$

where $v_\ell^{A'}$ and $a_\ell^{A'}$ are given in Sec. 2 of Ref. [44]. From Ref. [44] we know that $v_\ell^{A'}$ and $a_\ell^{A'}$ are the same for all the charged leptons and, thus, the only distinction in ε_ℓ between different flavors of leptons comes from μ_ℓ . As mentioned in Sec. IID, for light enough A' the axial coupling will be negligible and ε_ℓ is expected to be nearly independent of μ_ℓ , as is usually the case in models with dark photon. It is important to mention that, since Z' is also expected to be light, the dark photon experimental limits can also be applied as above with $A' \rightarrow Z'$ in Eq. (50) and $\{v_\ell^{A'}, a_\ell^{A'}\} \rightarrow \{v_\ell^{Z'}, a_\ell^{Z'}\}$ in Eq. (51). However, since A' is lighter by definition it is expected to be more strongly constrained.

There are several experiments with reported stringent limits for $m_{A'} > 1$ MeV [63–70]. The existing limits on ε_ℓ for a dark photon mass $m_{A'} > 1$ MeV are displayed on the top pane of Fig. 10 in Ref. [62].

D. Higgs Collider Data

1. Higgs Boson Mass

As aforementioned, h_1 is identified as the observed Higgs boson at the LHC. In this analysis, we take the mass of Higgs boson as $m_{h_1} = 125.10 \pm 0.14$ GeV [59].

2. Higgs Decays into Diphoton

The decay rate for $h_1 \rightarrow \gamma\gamma$ is given by

$$\Gamma(h_1 \rightarrow \gamma\gamma) = \frac{1}{64\pi} m_{h_1}^3 \left| F_{\gamma\gamma}(W^\pm) + F_{\gamma\gamma}(H^\pm) + \sum_{\text{Charged } f^{\text{SM}}} F_{\gamma\gamma}(f^{\text{SM}}) + \sum_{\text{Charged } f^{\text{H}}} F_{\gamma\gamma}(f^{\text{H}}) \right|^2, \quad (52)$$

where ²

$$F_{\gamma\gamma}(W^\pm) = \frac{-1}{16\pi^2} \cdot e^2 \cdot g \cdot \frac{1}{m_W} \cdot \cos\theta_1 \cdot [2 + 3\tau_W + 3\tau_W(2 - \tau_W)f(\tau_W)], \quad (53)$$

$$F_{\gamma\gamma}(H^\pm) = \frac{-1}{16\pi^2} \cdot e^2 \cdot g_{h_1 H^+ H^-} \cdot \frac{1}{m_{H^\pm}^2} \cdot \{\tau_{H^\pm} [1 - \tau_{H^\pm} f(\tau_{H^\pm})]\}, \quad (54)$$

$$F_{\gamma\gamma}(f^{\text{SM}}) = \frac{1}{16\pi^2} \cdot N_c \cdot e^2 Q_{f^{\text{SM}}}^2 \cdot \frac{4}{v} \cdot \cos\theta_1 \cdot \{\tau_{f^{\text{SM}}} [1 + (1 - \tau_{f^{\text{SM}}}) f(\tau_{f^{\text{SM}}})]\}, \quad (55)$$

$$F_{\gamma\gamma}(f^{\text{H}}) = \frac{-1}{16\pi^2} \cdot N_c \cdot e^2 Q_{f^{\text{H}}}^2 \cdot \frac{4}{v_\Phi} \sin\theta_1 \cdot \{\tau_{f^{\text{H}}} [1 + (1 - \tau_{f^{\text{H}}}) f(\tau_{f^{\text{H}}})]\}. \quad (56)$$

Here, and in what follows, we define $\tau_i = 4m_i^2/m_{h_1}^2$ where i indicates which particle is running inside the loop. N_c is the color factor, 1 for leptons and 3 for quarks. The coupling $g_{h_1 H^+ H^-}$ corresponds to the $h_1 H^+ H^-$ vertex and is given by

$$g_{h_1 H^+ H^-} = (2\lambda_H - \lambda'_H) v \cos\theta_1 - (\lambda_{H\Phi} + \lambda'_{H\Phi}) v_\Phi \sin\theta_1. \quad (57)$$

² Note that both the charged Higgs and heavy fermion contributions in $h_1 \rightarrow \gamma\gamma$ were not handled properly in [38].

The well-known loop function $f(x)$ is

$$f(x) = \begin{cases} \arcsin^2\left(\frac{1}{\sqrt{x}}\right) & (x \geq 1), \\ -\frac{1}{4} \left[\ln\left(\frac{1+\sqrt{1-x}}{1-\sqrt{1-x}}\right) - i\pi \right]^2 & (x < 1). \end{cases} \quad (58)$$

The signal strength parameter for the Higgs boson produced from the gluon-gluon fusion (ggH) can be obtained as

$$\mu_{\text{ggH}}^{\gamma\gamma} = \frac{\Gamma_h^{\text{SM}}}{\Gamma_{h_1}} \frac{\Gamma(h_1 \rightarrow gg)\Gamma(h_1 \rightarrow \gamma\gamma)}{\Gamma^{\text{SM}}(h \rightarrow gg)\Gamma^{\text{SM}}(h \rightarrow \gamma\gamma)}, \quad (59)$$

where the superscript SM refers to the SM Higgs boson h . The decay width of h_1 into two gluons is given by [38]

$$\Gamma(h_1 \rightarrow gg) = \frac{\alpha_s^2}{48\pi^3} m_{h_1}^3 \left| \sum_{q^{\text{SM}}} F_{gg}(q^{\text{SM}}) + \sum_{q^{\text{H}}} F_{gg}(q^{\text{H}}) \right|^2, \quad (60)$$

where

$$F_{gg}(q^{\text{SM}}) = \frac{\cos\theta_1}{v} \tau_{q^{\text{SM}}} \left[1 + (1 - \tau_{q^{\text{SM}}}) f(\tau_{q^{\text{SM}}}) \right], \quad (61)$$

$$F_{gg}(q^{\text{H}}) = -\frac{\sin\theta_1}{v_\Phi} \tau_{q^{\text{H}}} \left[1 + (1 - \tau_{q^{\text{H}}}) f(\tau_{q^{\text{H}}}) \right], \quad (62)$$

with q^{SM} and q^{H} refer to the SM quarks and the new colored fermions. The latest measurement of this signal strength is given by ATLAS as 0.96 ± 0.14 [71].

3. $h_1 \rightarrow \text{SM Fermions}$

The decay width of Higgs boson to SM fermions is given by

$$\Gamma(h_1 \rightarrow f^{\text{SM}} \bar{f}^{\text{SM}}) = \frac{N_c}{8\pi} \frac{m_{h_1} m_{f^{\text{SM}}}^2}{v^2} (1 - \tau_{f^{\text{SM}}})^{3/2} \cos^2\theta_1. \quad (63)$$

The signal strength for ggH production is then given by

$$\mu_{\text{ggH}}^{ff} = \cos^2\theta_1 \frac{\Gamma(h^{\text{SM}})}{\Gamma_{h_1}} \frac{\Gamma(h_1 \rightarrow gg)}{\Gamma^{\text{SM}}(h \rightarrow gg)}. \quad (64)$$

Note that this expression is independent of the fermion flavor and thus we compare against the best measured signal strength given by the decay into a pair of $\tau^+\tau^-$: $\mu_{\text{ggH}}^{\tau\tau} = 1.05_{-0.47}^{+0.53}$ [72].

4. Invisible Higgs Decay

If $m_{h_1} > 2m_{W'}$, the Higgs boson can decay invisibly into a pair of $W'^{(p,m)}$. The decay width of $h_1 \rightarrow W'^p W'^m$ is given by

$$\Gamma(h_1 \rightarrow W'^p W'^m) = \frac{g_H^4 (v \cos \theta_1 - v_\Phi \sin \theta_1)^2 m_{h_1}^3}{256\pi m_{W'}^4} \left(1 - \tau_{W'} + \frac{3}{4}\tau_{W'}^2\right) \sqrt{1 - \tau_{W'}}. \quad (65)$$

In our parameter choice, we will assume $2m_{\nu^H} > m_{h_1}$ so that h_1 does not decay into a pair of ν^H . The branching ratio of invisible Higgs decay is then given by

$$\text{BR}(h_1 \rightarrow \text{inv}) = \frac{\Gamma(h_1 \rightarrow W'^p W'^m)}{\Gamma_{h_1}}. \quad (66)$$

Recently, the ATLAS collaboration reported the most stringent constraint on the invisible decays of the Higgs produced via vector boson fusion. Assuming that the Higgs boson production cross section is comparable to the SM, the ATLAS collaboration set the limit $\text{BR}(h_1 \rightarrow \text{inv}) < 0.13$ at 95% C.L. [73].

IV. DARK MATTER CONSTRAINTS

A. Relic Density

The DM scenario presented here works similarly to the very well known WIMP DM. The DM candidate $W'^{(p,m)}$ begins in thermal equilibrium with the particle species in the hot primordial soup in the early universe before starting to freeze-out due to the expansion of the universe. The Boltzmann equation allows us to determine the evolution of the DM density and precisely determine the amount of relics that remain after freeze-out. This evolution is heavily influenced by the back and forth annihilation (creation) of pair of DM particles into (from) pairs of SM states in the early universe and their number densities. An excessive annihilation of DM into SM particles would result in very low relic density while not having enough annihilation would leave an overabundant DM. In our model, couplings between SM and BSM states have to be suppressed to minimize the effects on the precisely measured properties of the Z and the Higgs, given that these measurements are in good agreement with the SM.

The main DM annihilation channels in our model are to pairs of SM fermions mediated by Z and Z' as depicted in Fig. 1. Other annihilation channels are also possible but are far

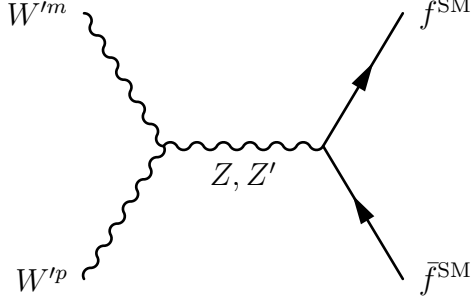


FIG. 1: Dominant annihilation channels of the $W'^{(p,m)}$ DM candidate.

more suppressed compared to the channels just mentioned. First, there is the A' exchange diagram. The A' couplings to SM fermions are suppressed by combinations of new gauge couplings in $v_f^{A'}$ and $a_f^{A'}$. Similar to the case of A' , the Z' couplings to the SM fermions are suppressed by its own $v_f^{Z'}$ and $a_f^{Z'}$. However, it is possible to have $m_{Z'}$ close to twice the mass of the $W'^{(p,m)}$, resulting in an important contribution from resonant annihilations. Secondly, we also have the h_1 and h_2 Higgs exchange diagrams. Their couplings to pairs of $W'^{(p,m)}$ and SM fermions are suppressed by g_H and light fermion masses m_q/v respectively. Finally, it is possible to have t -channel annihilation diagram via the exchange of a new heavy fermion, f^H , but this channel is suppressed by a factor of g_H on each of the two vertices of the diagram and by the mass of the heavy fermion in the propagator. The Feynman diagrams for the main annihilation processes as given in Fig. 1 can be computed straightforwardly and give rise to the following total cross section for each final fermion pair

$$\begin{aligned} \sigma(W'^p W'^m \rightarrow \bar{f} f) &= \frac{N_c g_M^2 g_H^2 m_{W'}^2}{72\pi s^2} \left(1 - \frac{4m_{W'}^2}{s}\right)^{1/2} \left(1 - \frac{4m_f^2}{s}\right)^{1/2} \left(\frac{s^2}{m_{W'}^4} + 20\frac{s}{m_{W'}^2} + 12\right) \\ &\times \left(\frac{(s - m_f^2)}{6m_{W'}^2} \mathcal{V}_+ + \frac{m_f^2}{2m_{W'}^2} \mathcal{V}_-\right), \end{aligned} \quad (67)$$

where

$$\begin{aligned} g_M &= \frac{\sqrt{g^2 + g'^2}}{2}, \quad \hat{\mathcal{D}}_k = 1 - \frac{m_k^2}{s} + i \frac{\Gamma_k m_k}{s}, \\ \mathcal{V}_\pm &= \mathcal{O}_{21}^2 \frac{v_f^2 \pm a_f^2}{|\hat{\mathcal{D}}_Z|^2} + \mathcal{O}_{22}^2 \frac{(v_f^{Z'})^2 \pm (a_f^{Z'})^2}{|\hat{\mathcal{D}}_{Z'}|^2} + 2\mathcal{O}_{22}\mathcal{O}_{21} (v_f v_f^{Z'} \pm a_f a_f^{Z'}) \operatorname{Re}\left(\frac{1}{\hat{\mathcal{D}}_Z \hat{\mathcal{D}}_{Z'}^*}\right). \end{aligned} \quad (69)$$

The annihilation mediated by the Z is suppressed by a factor of \mathcal{O}_{21}^2 required to be small mostly by measurements on the decay width of the Z and the decay branching fractions that limit the $Z \rightarrow W'^p W'^m$ process. As mentioned above, the channel mediated by the Z'

is also suppressed by combinations of gauge couplings that make most of the size of $v_f^{Z'}$ and $a_f^{Z'}$. However, these suppressions are not as strong as the suppression in other channels and when we include the effects from Z' resonance it is possible to bring the relic density to its expected value of $\Omega h^2 \sim 0.1$.

In our study, we will consider the measured value of $\Omega h^2 = 0.120 \pm 0.001$ as given by the Planck collaboration [49].

B. Direct Detection

Due to the small coupling between the DM candidate, $W'^{(p,m)}$, with the SM-like states h_1 and Z and the BSM states h_2 , Z' and A' which couple to the visible sector, it is possible to have effects from DM scattering against nucleons in detectors used in direct detection experiments. In this case, we have to consider the elastic scattering between a DM particle and the partons (both quarks and gluons) present in the nucleon. The suppression of vertices works in the same way as in the annihilation processes described in Sec. IV A, where h_j mediated processes are suppressed by a factor of $g_H^2 m_q^2 / v^2$ in the cross section with an additional $m_{h_j}^{-4}$ suppression from the propagator since these interactions happen via t -channel. Therefore, we are only left with the processes mediated by Z , Z' and A' in the t -channel. Usually, for direct detection processes the momentum exchange is considered to be very small and therefore t is expected to be small as well. This will result in amplitudes suppressed by the inverse squared of the mass of the mediator meaning that the light states, Z' and A' , will be less suppressed. In the approximation where the momentum exchange is smaller than the mass of the mediator, we can write the interaction between DM and light quark q as a contact interaction given by

$$\mathcal{L}_{\text{CI-DD}} = \sum_q \sum_{i=2}^3 \frac{g_M g_H \mathcal{O}_{2i} v_q^{Z(i)}}{2m_{Z(i)}^2} (W'^{p\mu} \partial_\nu W_\mu'^m - W'^{m\mu} \partial_\nu W_\mu'^p) \bar{q} \gamma^\nu q, \quad (70)$$

where $i = \{2, 3\}$ corresponds to $Z(2) \equiv Z'$ and $Z(3) \equiv A'$ respectively. It is worth noting that, as light as the mediators Z' and A' are, we can still integrate them out thanks to the comparably small maximum momentum transfer, q_{max} . The smallness of q_{max} is mostly due to W' being small as well. Consider $q_{\text{max}} \sim 2 v_{\text{DM}} m_{W'} m_A / (m_{W'} + m_A)$ with $m_{W'} = 0.5$ GeV and $v_{\text{DM}} = 10^{-3}$ c, and the target mass $m_A = 131$ GeV or 40 GeV for xenon or argon target respectively. In both cases $q_{\text{max}} \sim O(1 \text{ MeV})$ while we expect $m_{A'} \gtrsim O(10 \text{ MeV})$

due to constraints on dark photons. Additionally, smaller $m_{W'}$ results in even smaller q_{\max} . Furthermore, for the axial part of the interaction with the quark, in the small momentum exchange limit, only the space components of γ^ν remain but these components are suppressed by the $W'^{(p,m)}$ momentum due to the derivatives $\partial_\nu W'^{(p,m)}$ in Eq. (70) [74, 75]. This, together with axial couplings that are comparably much smaller than the vectorial ones results in an spin dependent cross section that is expected to be several orders of magnitude smaller than the spin independent one.

From Eq. (70), it is clear that the A' mediated process is expected to dominate the cross section unless $|\mathcal{O}_{23}/\mathcal{O}_{22}| < |m_{A'}/m_{Z'}|^2$. The case where both mediators participate equally is expected to happen only through fine tuning of masses and mixings. Therefore, we expect the cross section with the nucleons to be mostly mediated by either A' or Z' . The elastic cross section between $W'^{(p,m)}$ and a nucleon, N , is given by

$$\sigma_{W'N}^{\text{SI}} = \sigma_{W'p}^{\text{SI}} \frac{\sum_k \eta_k \mu_{A_k}^2 [Z_{\text{atom}} + (A_k - Z_{\text{atom}}) f_n / f_p]^2}{\sum_k \eta_k \mu_{A_k}^2 A_k^2}, \quad (71)$$

$$\sigma_{W'p}^{\text{SI}} = \frac{\mu_p^2 g_M^2 g_H^2 \mathcal{O}_{2i}^2}{4\pi m_{Z(i)}^4} f_p^2, \quad (72)$$

where $i = 2$ or 3 depending on the dominant mediator according to the discussion above, $\mu_p = m_{W'} m_p / (m_{W'} + m_p)$ is the reduced DM-proton mass, $\mu_{A_k} = m_{W'} m_{A_k} / (m_{W'} + m_{A_k})$ is the reduced DM-isotope nucleus mass and f_p and f_n are effective couplings of the DM with protons and neutrons, respectively. The atomic number is Z_{atom} and the isotope dependent variables η_k and A_k are the abundance and mass number of the k^{th} target isotope, respectively. Direct detection experiments usually report the number in Eq. (71) assuming isospin conservation, *i.e.*, $f_p = f_n$. In that case, it is straightforward to see that the ratio of the sums over isotopes reduces to 1 and $\sigma_{W'N}^{\text{SI}} = \sigma_{W'p}^{\text{SI}}$. However, in our case the couplings between quarks, u and d , and the gauge bosons, Z' and A' , are all different due to their distinct SM charges leading to isospin violation (ISV), *i.e.*, $f_p \neq f_n$. Following Refs. [76, 77], we can rescale the reported experimental limit, $\sigma_{\text{limit}} \rightarrow \sigma_{\text{limit}} \times \sigma_{W'p}^{\text{SI}} / \sigma_{W'N}^{\text{SI}}$ to account for ISV effects and use it to limit $\sigma_{W'p}^{\text{SI}}$ as given by Eq. (72). This rescaling depends on the mass of DM, the atomic numbers and the ratio f_n/f_p , and, therefore, will be different for different points in the parameter space.

To constraint the $W'^{(p,m)}$ -proton cross section we will use the most recent upper limits set by the experiments CRESST III [50], DarkSide-50 [51] and XENON1T [52].

C. Indirect Detection

Due to DM annihilation before freeze out happening through the resonance of an otherwise suppressed channel, the annihilation of DM in the present—after the shift in energy from the early to the current Universe—loses the resonance resulting in a very low annihilation cross section. We have checked that the value of the total annihilation cross section in G2HDM at the present time is of order 10^{-32} $\text{cm}^3\cdot\text{s}^{-1}$ or below, much lower than the canonical limits set for various channels by Fermi-LAT data [53, 54].

D. Mono-Jet

BP	$m_{W'}$ (GeV)	M_X (GeV)	m_{h_2} (TeV)	m_D (TeV)	m_{H^\pm} (TeV)	g_H (10^{-4})	g_X (10^{-4})	θ_1 (rad)	$\sigma_{pp \rightarrow W'pW'^mj}^{\text{precut}}$ (fb)
1	1.0	1.67	0.79	2.0	2.12	5.4	3.2	0.17	3.0
2	0.17	0.33	2.9	1.54	1.64	1.0	0.4	0.11	3.8

TABLE II: Parameters for the two benchmark points where the production cross section of the mono-jet signals with precuts are computed, as shown in the last column.

The occurrence of energetic jets with large missing transverse momentum has been searched by ATLAS [55, 56] and CMS [57] collaborations. However, the observed results are overall in agreement with the SM predictions and only exclusion limits have been reported. In our model, the process $pp \rightarrow W'^p W'^m j$ can give rise to mono-jet events at the LHC.

To analyze the mono-jet signal at the LHC, we choose two benchmark points (BPs) which are shown in Table II. These two BPs satisfy all theoretical, Higgs data and DM constraints. We evaluate the signal process cross section using `MadGraph 5` [78] with precuts for jets $p_T^j > 30$ GeV and $|\eta_j| < 2.8$, and for the missing transverse momentum $p_T^{\text{miss}} > 100$ GeV. It turns out the production cross sections with the precuts are about 3.0 fb and 3.8 fb for BP 1 and 2 respectively, and dominated by Z and Z' mediated diagrams. We generate 10^4 events for the $pp \rightarrow W'^p W'^m j$ process and recast ATLAS mono-jet search [56] using `MadAnalysis 5` [79]. The most sensitive signal region is found to be in the window $E_T^{\text{miss}} \in (700, 800)$ GeV (the signal region EM7 in Ref. [56]). The 95% C.L. exclusion limits on the production cross section are 400 fb and 680 fb for BP 1 and 2 respectively, which are much larger than the

signal expected from the model. Therefore, the LHC with luminosity of 139 fb^{-1} is not sensitive enough to search for mono-jet events from this model. However, the model can be probed by mono-jet searches at future hadron colliders such as the High-Luminosity Large Hadron Collider (HL-LHC) [80], the High-Energy Large Hadron Collider (HE-LHC) [81] and the Future Circular hadron-hadron Collider (FCC-hh) [82].

V. RESULTS

A. Methodology

The masses of the gauge bosons, m_Z , $m_{Z'}$ and $m_{A'}$, as well as the constraints from Sec. III are calculated through our own fortran codes, except for the Higgs invisible decay which can be calculated together with the DM constraints. The DM constraints of Sec. IV, in particular relic density, direct detection and indirect detection are calculated using `micrOMEGAs` [83] and a set of model files generated by `FeynRules` [84]. For the invisible decay branching ratio of the Higgs, we take advantage of the use of `CalcHEP` [85] within `micrOMEGAs` to calculate the decay width along with the rest of the DM constraints just mentioned.

All the points outside the theoretical constraints of Sec. III A are simply rejected. By the same token, the dark photon constraints are used to reject any parameter combination of $\varepsilon_{e,\mu}-m_{A'}$ or $\varepsilon_{e,\mu}-m_{Z'}$ located inside the currently excluded regions. The rest of the constraints in Sec. III are summed into a total χ^2 that also includes relic density and direct detection cross section. In the case of direct detection experiments, where a limit is reported at a 95% C.L. with null-signal assumption, we use a χ_{DD}^2 of the form

$$\chi_{\text{DD}}^2 = 4.61 \times \left(\frac{\sigma_{\text{theory}}}{\sigma_{\text{limit}}} \right)^2, \quad (73)$$

where the 4.61 factors allows $\chi_{\text{DD}}^2 = 4.61$ when we are exactly at the 95% C.L. of this two-dimensional limit.³ In mass ranges where more than one limit exists we take the one with the largest χ_{DD}^2 . Note that, due to ISV, the largest χ^2 for direct detection may not correspond to the experiment with the smallest cross section. Since direct detection limits

³ For a one-tailed test, the 95% C.L. corresponds to $\Delta\chi^2 = 2.71$ and $\Delta\chi^2 = 4.61$ of a Gaussian distribution in one and two dimensions, respectively. For a two-tailed test, the same numbers correspond to the 90% C.L. limit.

are reported assuming $f_p = f_n$ in Eq. (71), it is possible for ISV ($f_p \neq f_n$) to produce some amount of cancellation or enhancement of the limits depending on the atoms used in the detector. Calculating the cross section in the way described in Sec. IV B allows us to account for ISV and the atoms used in different experiments.

In the case of Higgs invisible decay branching fraction, where a limit is reported with a 95% C.L., the appropriate χ_{inv}^2 is given by

$$\chi_{\text{inv}}^2 = 2.71 \times \left(\frac{\text{BR}(h_1 \rightarrow \text{inv})}{0.13} \right)^2, \quad (74)$$

where, similarly to direct detection, the 2.71 factor allows for $\chi_{\text{inv}}^2 = 2.71$ when our result is exactly at the reported 95% C.L. in the one-dimensional case.

Parameter [units]	Range
m_{h_1} [GeV]	[124.26, 125.94]
m_{h_2} [TeV]	[0.3, 10]
m_D [TeV]	[0.3, 10]
m_{H^\pm} [TeV]	[0.3, 10]
θ_1 [rad]	$[-\pi/2, \pi/2]$
$\log_{10}(m_{W'}/\text{GeV})$	$[-3, 2]$
$\log_{10}(M_X/\text{GeV})$	$[-3, 2]$
$\log_{10}(g_H)$	$[-6, 0]$
$\log_{10}(g_X)$	$[-6, 0]$
m_{fH} [TeV]	3 (fixed)

TABLE III: Ranges and values for the prior of the parameters used in this analysis. All priors are taken as uniform inside their ranges for the parameters listed in the table. While the m_{h_1} range in this table corresponds to the measured $\pm 6\sigma$ interval, `emcee` takes care of sampling it according to the result of the total χ^2 .

To sample the parameter space we use the affine invariant Markov Chain Monte Carlo (MCMC) ensemble sampler `emcee` [86] which presents advantages such as fast calculation of parameter distributions in several dimensions. The initial prior and ranges of each parameter are contained in Table III. In particular, the parameters $m_{W'}$, M_X , g_H and g_X are scanned in base-10 logarithmic scale. This is mostly because we expect these parameters to be small

but different from zero and that their effects depend heavily on their orders of magnitude. For the masses of the heavy fermions, we expect their contributions to be heavily suppressed by the requirement that $m_{fH} = \mathcal{O}(1 \text{ TeV})$. Therefore we consider all of them degenerated with a mass of $m_{fH} = 3 \text{ TeV}$ putting them safely above any current search for heavy fermionic states. The rest of the parameters are scanned with a uniform prior in linear scale. To guarantee that our final distributions are independent of the initial points we perform several small runs collecting $\mathcal{O}(10^4)$ points for each run using $\mathcal{O}(100)$ walkers. The initial points for the walkers are always allowed by theoretical and dark photon constraints but otherwise random inside the prior. After checking that the final distributions are consistent between different runs, we perform a large scan with 300 walkers collecting 160,000 points after burn-in and thinning.

B. Numerical Results

We present the numerical results for visualization in Figs. 2–5. To follow the discussion below more smoothly, we suggest our readers to read the captions of these figures first and then view and compare them in parallel.

The most notable feature of both panes of Fig. 2 is the band-shaped allowed region. In the case of $(m_{W'}, g_H)$ plane shown in the left pane, the band is caused by the relation between relic density and cross section, $\Omega h^2 \propto 1/\langle\sigma v\rangle$. Considering that we have $\sigma \propto g_H^2 m_{W'}^2/s^2$ from Eq. (67), assuming $s \sim 4 m_{W'}^2$, we have that $g_H^2 m_{W'}^2/s^2 \sim g_H^2/(16 m_{W'}^2)$ resulting in $\Omega h^2 \propto m_{W'}^2/g_H^2$. This means that to keep a constant relic density, $m_{W'}$ and g_H have to keep a linear relationship as displayed in the left pane of Fig. 2. Deviations from this band result in the relic density going either above or below the value measured by the Planck satellite.

In the case of the right pane of Fig. 2, the band can be explained by the possibility of having a resonant annihilation of $W'^{(p,m)}$ mediated by the Z' . First note that Eq. (23) directly relates $m_{A'}$ and M_X and, as can be seen in the right pane of Fig. 3, $m_{A'}$ is required to be mostly below 0.2 GeV due to the LHCb results, thus limiting also the size of M_X . Then, from Eq. (22) we know that the term with $m_{W'}^2$ factor dominates over the term with M_X^2 . Finally, resonant annihilation is achieved for $m_{Z'} \approx 2 m_{W'}$ meaning $1 + 4g_X^2/g_H^2 \approx 4$ or $g_X^2/g_H^2 \approx 3/4$, resulting in the band seen in the right pane of Fig. 2. Again, large deviations from this band result in too much or not enough annihilation to achieve the correct relic

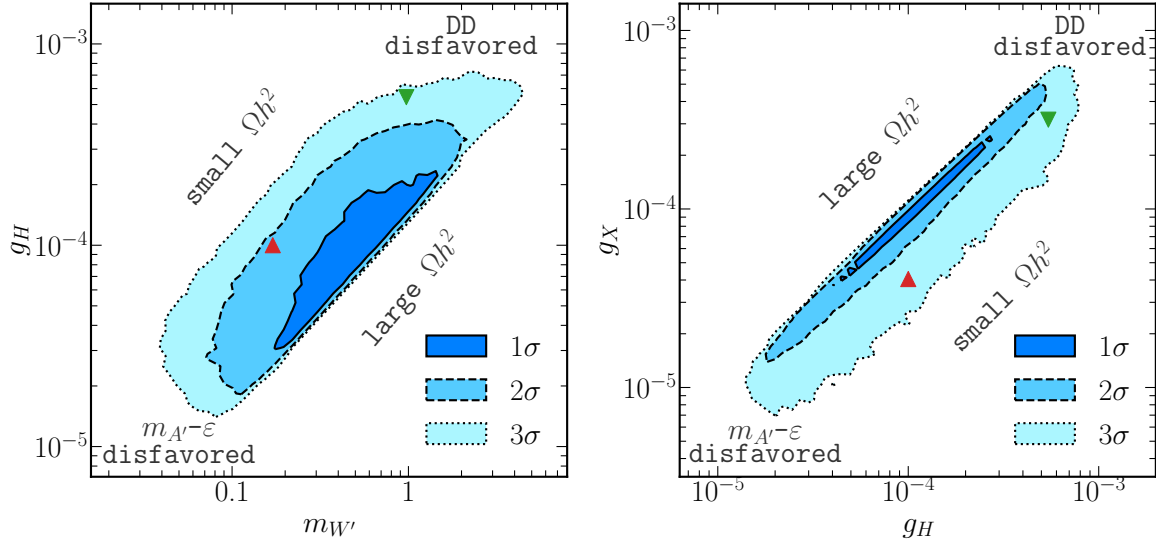


FIG. 2: The 1σ , 2σ and 3σ allowed regions (dark blue, medium blue and light blue, respectively) projected on the planes $(m_{W'}, g_H)$ (left) and (g_H, g_X) (right). The solid, dashed and dotted black contours delimit the 1σ , 2σ and 3σ regions respectively. The labels on empty zones represent the most relevant constraint in that region. The mono-jet benchmark points of Sec. IV D are shown as a green down-triangle (BP 1) and a red up-triangle (BP 2).

density. Due to this g_X - g_H correlation, the two-dimensional allowed regions in Fig. 4 for all the distributions involving g_X and g_H have similar shapes. Here it is important to mention that exact resonance, $m_{Z'} = 2m_{W'}$, would result in too much annihilation and, therefore, in Ωh^2 well below Planck's measurement.

Besides their band-shaped tendency, both panes in Fig. 2 are bounded in their top-right and bottom-left corners by the DM direct detection and dark photon constraints, respectively. We know that the direct detection cross section grows with g_H^2 as seen in Eq. (72), therefore, it is expected to see it setting an upper bound on g_H . Furthermore, as can be seen in the left pane of Fig. 3, direct detection experiments practically create a wall that limits the size of $m_{W'}$ from above. The effects of this limit are reflected in the upper bound of $m_{W'}$ in the left pane of Fig. 2. In the case of the region disfavored by dark photon searches, this is mostly due to the ν -CAL I experiment limiting ε from below as seen in the right pane (olive green shaded zone) of Fig. 3. The ε coupling limit is passed to g_H through the vectorial and axial couplings $v_f^{A'}$ and $a_f^{A'}$ that depend on it, resulting on the lower limit on g_H that can be seen in both panes of Fig. 2.

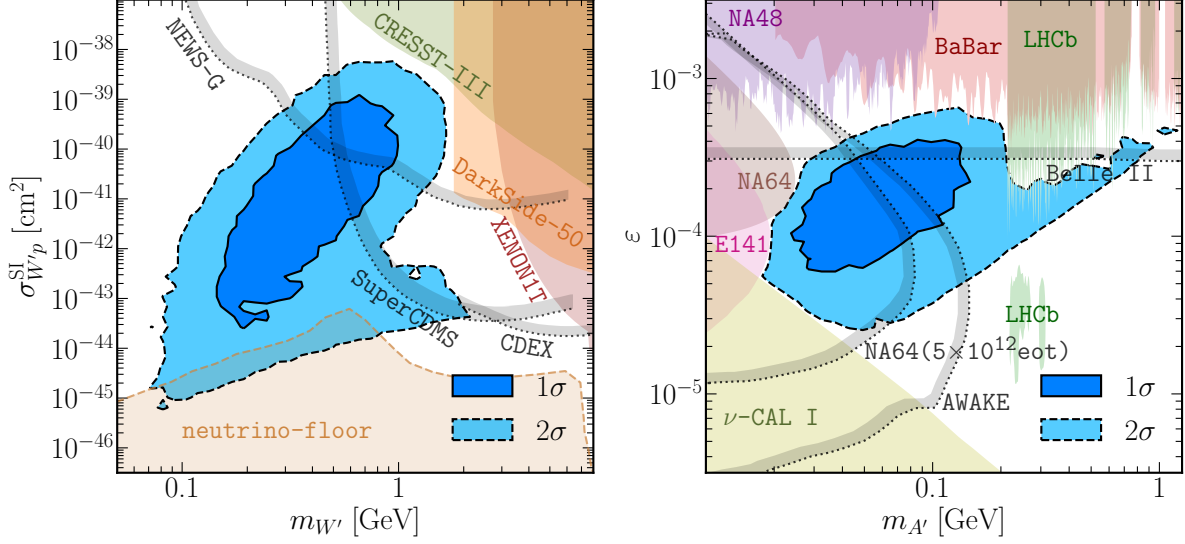


FIG. 3: The 1σ and 2σ allowed contours projected on the DM mass, $m_{W'}$, vs. direct detection cross section (left) and dark photon mass, $m_{A'}$, vs. ε coupling (right). The experimental excluded regions used in this study are shown as solid colored regions. Projected experimental limits are shown as dotted lines, with the direction of the exclusion marked in gray. In the case of direct detection (left), the limit set by the neutrino floor is shown as a dashed light orange line.

In the left pane of Fig. 3 we show the allowed region projected on the $(m_{W'}, \sigma_{W'p}^{SI})$ plane, where $\sigma_{W'p}^{SI}$ is the cross section for spin-independent scattering on a proton. The dark (light) blue shaded zone represents the 1σ (2σ) allowed region. The current DM direct detection measurements from CRESST III (green) [50], DarkSide-50 (orange) [51] and XENON1T (brown) [52] constrain the DM mass to remain below ~ 2 GeV. A small part of the 2σ allowed region lies below the neutrino floor (light orange), where the coherent neutrino-nucleus scattering would dominate over any DM signal. Additionally, we show that experiments in the near future such as NEWS-G [87], SuperCDMS [88] and CDEX [89] can further probe our allowed parameter space, in particular for $m_{W'} \gtrsim 0.3$ GeV with NEWS-G and down to $\sigma_{W'p}^{SI} \sim 10^{-44}$ cm² with SuperCDMS and CDEX.

The right pane in Fig. 3 shows the allowed region projected on the $(m_{A'}, \varepsilon)$ plane with the coupling $\varepsilon \equiv \varepsilon_\ell$. Various experimental limits from dark photon searches are displayed in color shaded zones including LHCb (green) [63], BaBar (pink) [64], NA48 (purple) [65], NA64 (light brown) [66], E141 (magenta) [67] and ν -CAL I (light green) [68, 69]. The dilepton searches at the LHCb, BaBar and NA48 put upper limits of $\varepsilon \lesssim 10^{-3}$ for $m_{A'} \gtrsim 0.03$ GeV,

especially LHCb which sets a strong limit on ε at $0.2 \text{ GeV} < m_{A'} < 0.5 \text{ GeV}$ causing a concave region in the 2σ allowed region at this mass range. We note that this concave region due to LHCb corresponds to the concave region at $(m'_{W'}, \sigma_{W'p}^{\text{SI}}) \sim (1 \text{ GeV}, 10^{-42} \text{ cm}^2)$ in the left pane of the same figure. The LHCb long lived dark photon search constraints [63] are also shown by the two isolated green shaded islands around ε equals 2×10^{-5} . On the other hand, the beam dump experiments NA64, E141 and ν -CAL I close the available space for smaller ε and lighter $m_{A'}$ setting lower bounds of $m_{A'} > 0.02 \text{ GeV}$ and $\varepsilon \gtrsim 2 \times 10^{-5}$. The lower limit on ε for $m_{A'} > 0.05 \text{ GeV}$ is due to the DM relic density measured by the Planck experiment. Interestingly, our final allowed region is located in the gap between the beam-dump and the collider based experiments, an area of special interest for future dark photon searches. For example, Belle-II [90] with a luminosity of 50 ab^{-1} can probe ε down to 2×10^{-4} , the next upgrade of NA64 [91] can cover $10^{-5} \lesssim \varepsilon \lesssim 10^{-3}$ and $m_{A'} \lesssim 0.08 \text{ GeV}$ by reaching $\sim 5 \times 10^{12}$ electrons-on-target (abbreviated by eot in the figure) and Advanced WAKEfield Experiment (AWAKE) run 2 [92] can reach $m_{A'}$ up to 0.15 GeV with 10^{16} electrons-on-target with an energy of 50 GeV . These limits are shown explicitly in the right pane of Fig. 3 as dotted lines with the side of the exclusion in gray. In the future, with access to high energy electron-proton colliders, AWAKE may reach 1 TeV for the electrons, extending $m_{A'}$ up to 0.6 GeV [92] and dark photon searches at LHeC and FCC-he [93] may even cover our entire allowed parameter space.

We present two-dimensional projections of the allowed region for our BSM parameters in Fig. 4. The dark, light and lighter blue zones indicate the 1σ , 2σ and 3σ allowed regions respectively. One important thing to note is that the m_{h_2} , m_D and m_{H^\pm} masses show an apparent upper bound at 1σ and 2σ . This upper bound actually depends on the maximum value chosen for the prior of these three parameters and has no physical meaning. In the case of m_{h_2} , the apparent limit is due to the reduced θ_1 for large m_{h_2} seen in the (m_{h_2}, θ_1) subfigure while for m_D and m_{H^\pm} it is due to their near degeneracy shown in the (m_D, m_{H^\pm}) subfigure. We have checked that changing the maximum scanned value for these three parameters does not change the rest of the distributions, except for θ_1 where, understandably, larger m_{h_2} sharpens the peak at $\theta_1 = 0$ where $h_1 = h_{\text{SM}}$ exactly. The near degeneracy for m_D and m_{H^\pm} is due to their comparably small mass squared difference $m_D^2 - m_{H^\pm}^2 = v^2(\lambda'_{H\Phi} + \lambda'_H)/2$. Given that $(\lambda'_{H\Phi} + \lambda'_H)/2$ is bounded by unitarity constraints, the mass squared difference is expected to remain $\mathcal{O}(v^2)$ or less, meaning that as m_D and m_{H^\pm} grow away from v their

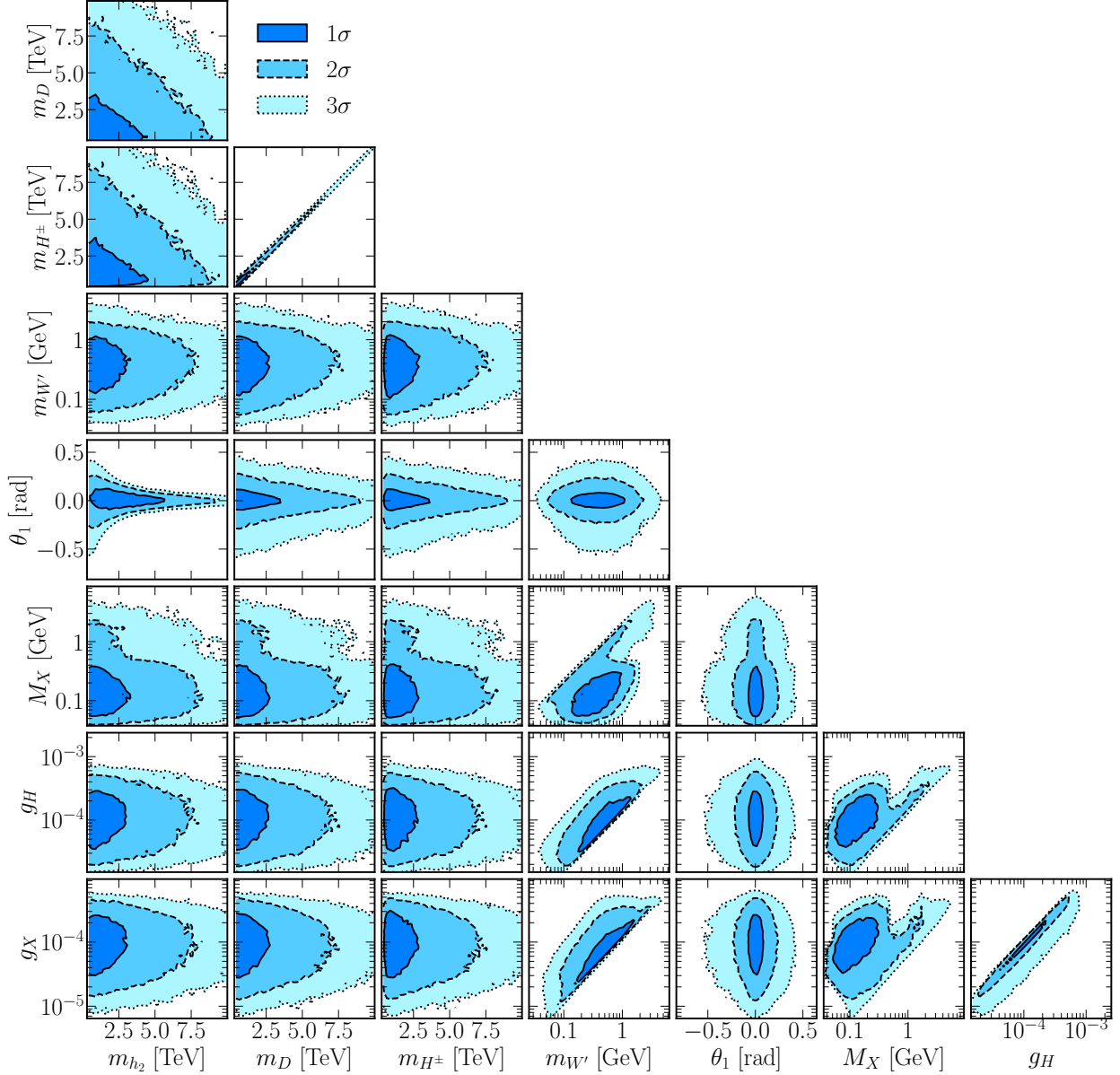


FIG. 4: Marginalized distributions in two dimensions for the parameters scanned in this study. The 1σ , 2σ and 3σ regions are marked in dark, light and lighter blue delimited by solid, dashed and dotted lines, respectively.

proportional difference rapidly grows smaller. Their near degeneracy is also noticeable in all their two-dimensional distributions since the distributions become nearly identical as m_D and m_{H^\pm} grow larger.

Another interesting feature is that the charged Higgs mass distributions reveal the presence of a lower limit around $m_{H^\pm} \approx 400$ GeV where the contours show that the distribution

falls rapidly. This is due to the constraint from the Higgs decays into diphoton as shown in Eq. (52). Moreover, due to the relation between M_X and $m_{A'}$ that can be inferred from Eq. (23), the distributions in the (M_X, g_X) and (M_X, g_H) subfigures (second column from the right in (Fig. 4)) are close to the distribution shown for the dark photon constraint in the right pane of Fig. 3.

We present the marginalized one-dimensional distributions for the most relevant parameters in Fig. 5 together with their central values and their 1σ intervals. As mentioned before, there is a relation between g_X and g_H which is seen again in their marginalized distributions in the top two panes since both peak close to 10^{-4} and have very similar 1σ intervals. The distribution for $\log_{10}(M_X/\text{GeV})$ in the middle-left pane shows the effects of the LHCb constraint around $\log_{10}(M_X/\text{GeV}) \approx 0$ and peaks just above -1 . Because of the precise measurements on the Higgs properties at the LHC, the mixing angle between h_1 (identified to be the observed 125 GeV Higgs) and h_2 , θ_1 is found to have a 1σ interval of $(-9.8, 9.5) \times 10^{-2}$ rad as shown in the middle-right pane of Fig. 5. For the distribution of the DM mass $m_{W'}$ in the bottom pane, we have the 1σ interval for $\log_{10}(m_{W'}/\text{GeV})$ between -0.81 and -0.04 which corresponds to $m_{W'} \in [0.15, 0.91]$ GeV peaking at $m_{W'} \approx 0.39$ GeV.

After the above long discussions of our numerical analysis, perhaps a high level summary is useful.

- We have focused our numerical analysis on the parameter space of the model that can lead to a sub-GeV $W'^{(p,m)}$ DM with a mass range of MeV–GeV.
- The viable domains of the parameter space are summarized in Fig. 4, where the 1 – 3σ contours allowed by all existing experimental constraints are shown for any combination of two of the 8 free parameters while the rest of the parameters are marginalized. All the masses of the new heavy fermions in the model, required by anomaly cancellation, are set at 3 TeV. For the two cases of $(m_{W'}, g_H)$ and (g_H, g_X) , more detailed information on the boundaries of the contours due to the different constraints imposed are exhibited in Fig. 2.
- It is both clear and exciting to see from the allowed 1σ and 2σ contours on the plane of $m_{W'}$ versus $\sigma_{W'p}^{\text{SI}}$ displayed in the left pane of Fig. 3 that future experiments like NEWS-G and SuperCDMS can put more stringent constraints on the model. Indeed, about $1/3$ of the current viable parameter space in the $(m_{W'}, \sigma_{W'p}^{\text{SI}})$ plane would be

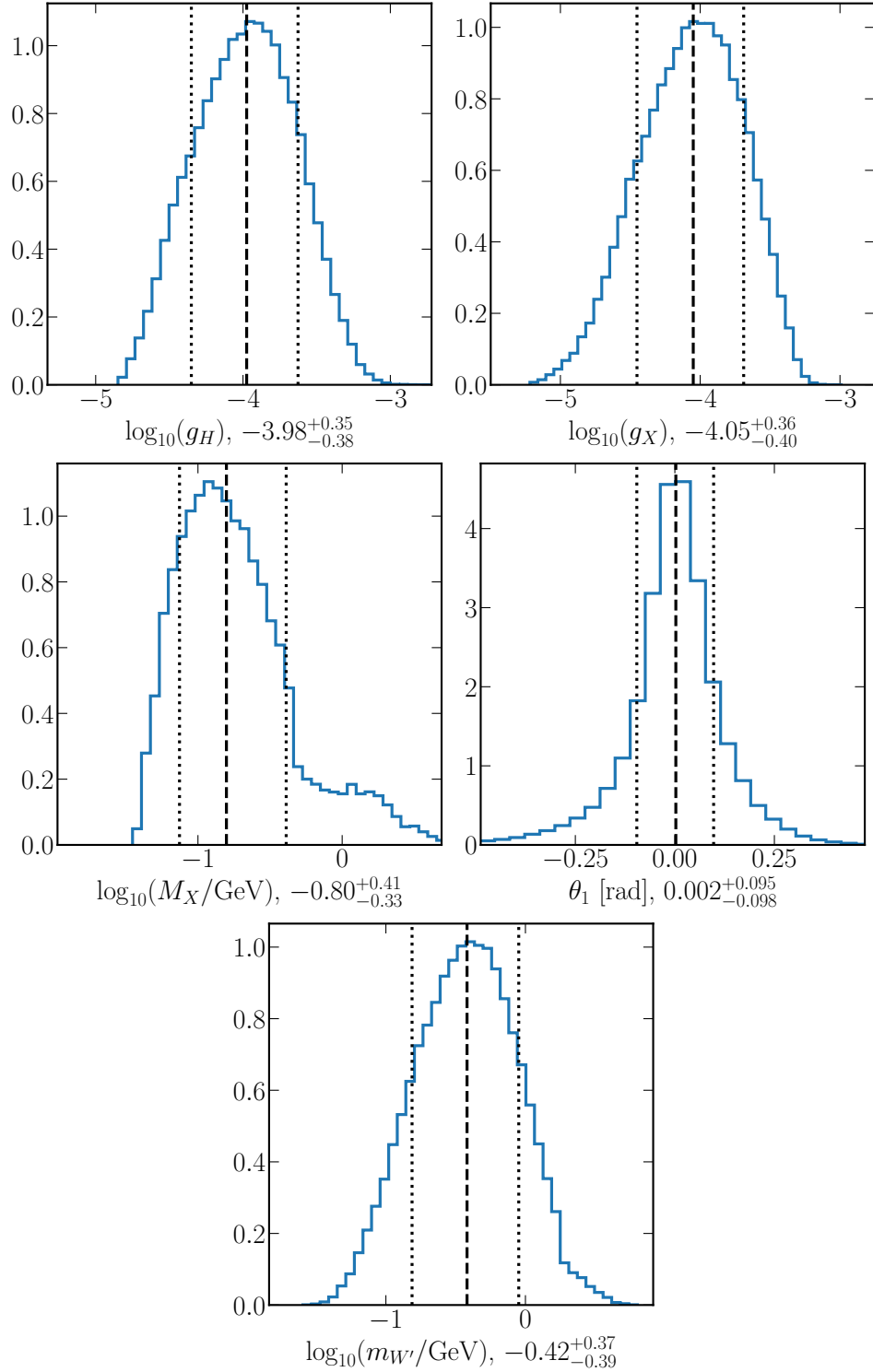


FIG. 5: Marginalized distributions of the most relevant parameters used in this study. Central values are indicated in the x -axis label. Since all the distributions are normalized, the y -axis values are only for reference.

facing challenge. On the other hand, the region where the projected CDEX sensitivity can reach is already disfavored in G2HDM. Note that a small portion of the 2σ allowed parameter space in the $(m_{W'}, \sigma_{W'p}^{\text{SI}})$ plane is overlapping with the neutrino floor.

- For the allowed contours of dark photon coupling ε and mass $m_{A'}$ exhibited in the right pane of Fig. 3, future upgraded NA64 experiment with 5×10^{12} electrons-on-target, proof-of-principle experiment AWAKE run 2 with 10^{16} electrons-on-target, and next generation B-factory experiment Belle II would probe more than 1/2 of the current viable domain in the $(m_{A'}, \varepsilon)$ plane.
- The correlation between the DM and dark photon physics and their constraints in G2HDM exhibited in the left and right panes of Fig. 3 is rather novel and interesting. Indeed any non-abelian vector DM is likely accompanied by at least one extra neutral gauge boson which can play the role of Z' or A' . Thus considerations of experimental constraints for both DM and dark photon physics must be taken into account mandatory. Although our analysis is performed in the context of a specific model, we expect some of the features obtained in this work may be generic for any low mass non-abelian vector DM with a dominated vector portal of neutral gauge boson communicating to the SM sector. Perhaps we may be entertained by *nature* revealing to us not only a low mass dark matter W' but also a dark photon and a dark Z' with nearby masses. These are the three gauge bosons associated with the dark $SU(2)_H \times U(1)_X$ sector, in mirror with the visible SM gauge group $SU(2)_L \times U(1)_Y$. Due to the minuscule couplings of g_H and g_X , direct detections of the dark matter, dark photon and dark Z' (as well as other new particles introduced in G2HDM) at colliders would belong to the lifetime frontier and high luminosity/energy frontier at the upgrade of LHC and future colliders.

VI. CONCLUSION

In this work, we studied a simplified version of the G2HDM [38]. In previous works, it was demonstrated that the original G2HDM successfully explains dark matter while keeping a parameter space consistent with theoretical and experimental expectations [39, 43, 44]. The simplifications considered in this study reduced the size of the scalar potential and the parameter space by removing the scalar $SU(2)_H$ triplet. Thankfully, the absence of this triplet does not affect the h -parity and another dark sector particle, the $W'^{(p,m)}$, steps up as a DM candidate. For the properties of $W'^{(p,m)}$ we settled on exploring the sub-GeV mass range. Interestingly, in this region the extra vector states Z' and A' happen to have relevant roles as mediators for the annihilation and direct detection processes of the DM. In particular, reaching the appropriate amount of annihilation to have the correct relic density would have been difficult if not impossible without the channel mediated by the Z' .

We started with the usual theoretical checks on the scalar potential ensuring that the minimum is stable and that the couplings remain unitary at tree level. Given that the LHC has been closing in on the detailed properties of the 125 GeV Higgs, we check that our scalar sector provides a particle, h_1 , that matches the mass and decays that have been measured. The same can be said in the case of the gauge sector and the Z with its properties already very well measured at LEP. In the case of the light Z' and A' we constrained their interactions with SM leptons by checking against the regions excluded by dark photon searches in LHCb, BaBar, NA48, NA64, E141 and ν -CAL I. Finally, we required our DM candidate, $W'^{(p,m)}$, to have the correct relic density measured by Planck satellite with a spin-independent direct detection cross section below the limits found by CRESST-III, DarkSide-50 and XENON1T.

In our numerical analysis, we uncovered some interesting features of the parameter space, such as a correlation between the couplings g_H and g_X with superweak size $O(10^{-5} - 10^{-3})$ and that most of our results lie inside the gap between various dark photon explorations. The latter becomes more important when we consider that this gap is projected to be further explored in the future with the upgrades to NA64 and AWAKE and the B-factory Belle II. This would reduce the allowed parameter space nearly by half, and therefore remove a good portion of our allowed parameter space in the lighter A' region. Moreover, future DM direct detection experiments like NEWS-G and SuperCDMS may reduce the parameter space by exploring the regions with heavier $W'^{(p,m)}$ and larger cross section.

To summarize, we found that the simplified G2HDM developed in this work provides a viable vector DM candidate with mass down to $\mathcal{O}(10^{-2})$ GeV. All the predictions in the scalar and gauge sectors are in good agreement with current observations. Importantly, both new vector states, Z' and A' , play key roles for DM observables. Besides the possibility of detecting the $W'^{(p,m)}$ in DM direct detection experiments, the dark photon, A' , is predicted to be well positioned for future observations that may reach $m_{A'} \sim 0.1$ GeV. This work demonstrates that the G2HDM is not only a successful and competitive dark matter formulation but can also serve as a starting point with diverse exploration possibilities.

Acknowledgments

The analysis presented here was done using the resources of the high-performance T3 Cluster at the Institute of Physics, Academia Sinica. This work is supported in part by the Ministry of Science and Technology of Taiwan under Grants No. 108-2112-M-001-046 (TCY) and No. 109-2811-M-001-595 (RR) and by National Natural Science Foundation of China under Grants No. 11775109 (VQT). VQT would like to thank the Institute of Physics, Academia Sinica, Taiwan for its hospitality during this work.

Appendix A: Mass Spectra of Goldstone Bosons and Gauge Fixings in General Renormalizable Gauge

In Sec. IIC as well as in all previous works, we have derived the scalar and vector boson mass spectra in the 't Hooft-Landau gauge in which all the gauge parameter parameters ξ s were set to zero. This hides away the issue of gauge dependence and all the Goldstone bosons are massless. Since the physical dark Higgs D is a linear combination of H_2^{0*} in the inert doublet H_2 and Goldstone boson G_H^p in the hidden doublet Φ_H , one might wonder what would happen in the general renormalizable gauge. We take the opportunity here to examine this question more carefully and discuss the related issue of gauge mixings in G2HDM.

1. G^\pm and $G_H^{(p,m)}$

First G^\pm . This is the same as in SM, which after SSB the covariant kinetic term of the Higgs field H_1 contains the following mixing term

$$-\frac{i}{2}gvW_\mu^+\partial^\mu G^- + \text{H.c.} \quad (\text{A1})$$

In the general renormalizable gauge, one introduces the following gauge fixing term

$$-\frac{1}{\xi_W}\left|\partial^\mu W_\mu^+ - \frac{i}{2}\xi_W gvG^+\right|^2, \quad (\text{A2})$$

where ξ_W is an arbitrary gauge parameter. Expanding out Eq. (A2), up to a total derivative, it will cancel the mixing term in Eq. (A1). In addition, it will modify the W^\pm -boson propagator to be ξ_W -dependent whose form is well known in the literature, and the Goldstone boson G^\pm (absorbed by the longitudinal component of W^\pm) will develop a mass equals to $gv\sqrt{\xi_W}/2$.

The story of $G_H^{(p,m)}$ in G2HDM is a little bit more interesting. The mixing term contains two contributions coming from the covariant kinetic terms of the H_2 and Φ_H fields

$$-\frac{i}{2}g_H W_\mu^p (v_\Phi \partial^\mu G_H^m - v \partial^\mu H_2^0), \quad (\text{A3})$$

which indicates that the physical Goldstone field \tilde{G}_H^p (\tilde{G}_H^m) is actually a linear combination of H_2^{0*} (H_2^0) and G_H^p (G_H^m), *viz.*

$$\tilde{G}_H^p = \frac{1}{\sqrt{v^2 + v_\Phi^2}} (v_\Phi G_H^p - v H_2^{0*}), \quad \tilde{G}_H^m = \frac{1}{\sqrt{v^2 + v_\Phi^2}} (v_\Phi G_H^m - v H_2^0). \quad (\text{A4})$$

$\tilde{G}_H^{(p,m)}$ are absorbed by the longitudinal components of $W'^{(p,m)}$. The other physical orthogonal combination is the complex dark Higgs D

$$D = \frac{1}{\sqrt{v^2 + v_\Phi^2}} (vG_H^p + v_\Phi H_2^{0*}) , \quad D^* = \frac{1}{\sqrt{v^2 + v_\Phi^2}} (vG_H^m + v_\Phi H_2^0) . \quad (\text{A5})$$

In analogous with Eqs. (A1) and (A2), to cancel the mixing term in Eq. (A3) one introduces the following general gauge fixing term

$$-\frac{1}{\xi_{W'}} \left| \partial^\mu W_\mu^p - \frac{i}{2} \xi_{W'} g_H \tilde{v} \tilde{G}_H^p \right|^2 , \quad (\text{A6})$$

where $\xi_{W'}$ is an arbitrary gauge parameter and $\tilde{v} = \sqrt{v^2 + v_\Phi^2}$. As in the case of W^\pm , the propagator of $W'^{(p,m)}$ is then get modified under this general renormalizable gauge. The mass matrix $\mathcal{M}_{S'}^2$ in Eq. (12) is also modified as

$$\mathcal{M}_{S'}^2 = \begin{pmatrix} \frac{1}{2} \lambda_{H\Phi} v^2 + \frac{1}{4} \xi_{W'} g_H^2 v_\Phi^2 & \frac{1}{2} \lambda'_{H\Phi} v v_\Phi - \frac{1}{4} \xi_{W'} g_H^2 v v_\Phi \\ \frac{1}{2} \lambda'_{H\Phi} v v_\Phi - \frac{1}{4} \xi_{W'} g_H^2 v v_\Phi & \frac{1}{2} \lambda'_{H\Phi} v_\Phi^2 + \frac{1}{4} \xi_{W'} g_H^2 v^2 \end{pmatrix} , \quad (\text{A7})$$

which has two eigenvalues $g_H^2 \xi_{W'} \tilde{v}^2 / 4$ and $\lambda'_{H\Phi} \tilde{v}^2 / 2$. The first one is the mass-squared of the Goldstone boson $\tilde{G}_H^{(p,m)}$ in the general gauge, while the second one is the mass-squared of the complex dark Higgs D which is the same as Eq. (16) previously derived from the 't Hooft-Landau gauge as it should!

2. G^0 , G_H^0 and \mathcal{S}

Similarly for the neutral gauge bosons, after SSB, we have the following mixing terms from the covariant kinetic terms of the H_1 and Φ_H fields

$$\begin{aligned} & -\frac{1}{2} v (g' B^\mu - g W^{3\mu} + g_H W'^{3\mu} + 2g_X X^\mu) \partial_\mu G^0 \\ & + \frac{1}{2} v_\Phi (g_H W'^{3\mu} - 2g_X X^\mu) \partial_\mu G_H^0 . \end{aligned} \quad (\text{A8})$$

For the $U(1)_X$ gauge field, we also use the Stueckelberg mechanism to provide a mass. The Stueckelberg Lagrangian is

$$\begin{aligned} \mathcal{L}_{\text{St}} &= \frac{1}{2} (\partial^\mu \mathcal{S} + M_X X^\mu)^2 , \\ &= \frac{1}{2} (\partial^\mu \mathcal{S})^2 + \frac{1}{2} M_X^2 X^\mu X_\mu + M_X X^\mu \partial_\mu \mathcal{S} . \end{aligned} \quad (\text{A9})$$

Here \mathcal{S} and M_X are the Stueckelberg field and mass respectively. The middle term gives X a mass M_X , while the last term indicates the mixing of \mathcal{S} with the longitudinal component of X^μ . Note that \mathcal{S} is massless.

Recall that the first two terms in Eq. (A8) are SM-like and they can be combined as

$$(g'B_\mu - gW_\mu^3) = -(g' \sin \theta_W + g \cos \theta_W) Z_\mu^{\text{SM}}. \quad (\text{A10})$$

Thus the total mixing terms including both Eq. (A8) and the last term in Eq. (A9) are

$$\begin{aligned} & + \frac{1}{2}v [(g' \sin \theta_W + g \cos \theta_W) Z^{\text{SM}\mu} - g_H W'^{3\mu} - 2g_X X^\mu] \partial_\mu G^0 \\ & + \frac{1}{2}v_\Phi (g_H W'^{3\mu} - 2g_X X^\mu) \partial_\mu G_H^0 + M_X X^\mu \partial_\mu \mathcal{S}. \end{aligned} \quad (\text{A11})$$

Note that, as one would expect, the photon field A^μ doesn't enter in Eq. (A11) which is coming entirely from SSB and Stueckelberg mechanism. The photon field remains massless, it has no associated Goldstone boson and its general gauge fixing term is simply given by $-(\partial_\mu A^\mu)^2 / 2\xi_\gamma$ as in the SM case. So does the massless gluon field, whose gauge fixing term is $-(\partial_\mu A^{a\mu})^2 / 2\xi_g$ where $a = 1, \dots, 8$ is the adjoint index of the color group $SU(3)_C$.

As mentioned in the text, the neutral vector gauge bosons Z^{SM} , W'^3 and X are in general mixed together according to

$$\begin{pmatrix} Z^{\text{SM}} \\ W'^3 \\ X \end{pmatrix} = \mathcal{O} \cdot \begin{pmatrix} Z_1 \\ Z_2 \\ Z_3 \end{pmatrix}, \quad (\text{A12})$$

where \mathcal{O} is an orthogonal matrix. In our numerical scan of the parameter space in this work, we have $Z_1 = Z \simeq Z^{\text{SM}}$ which is very close to the SM Z -boson, and $Z_2 = Z'$ and $Z_3 = A'$, both of which are lighter than the Z . We will use Z_i in this appendix instead of Z , Z' and A' .

In terms of the physical fields Z_i , Eq. (A11) becomes

$$\begin{aligned} & + \frac{1}{2}v [(g' \sin \theta_W + g \cos \theta_W) \mathcal{O}_{1i} Z_i^\mu - g_H \mathcal{O}_{2i} Z_i^\mu - 2g_X \mathcal{O}_{3i} Z_i^\mu] \partial_\mu G^0 \\ & + \frac{1}{2}v_\Phi (g_H \mathcal{O}_{2i} Z_i^\mu - 2g_X \mathcal{O}_{3i} Z_i^\mu) \partial_\mu G_H^0 + M_X \mathcal{O}_{3i} Z_i^\mu \partial_\mu \mathcal{S} \\ & \equiv \sum_{i=1}^3 Z_i^\mu \partial_\mu G_i. \end{aligned} \quad (\text{A13})$$

Here we have defined three physical Goldstone fields absorbed by the longitudinal components of the three physical Z_i as

$$G_i = \tilde{C}_{i1} G^0 + \tilde{C}_{i2} G_H^0 + \tilde{C}_{i3} \mathcal{S} \quad (i = 1, 2, 3), \quad (\text{A14})$$

where the coefficients \tilde{C}_{ij} can be read off from the first two lines in Eq. (A13), namely

$$\tilde{C}_{i1} = \frac{1}{2}v [(g' \sin \theta_W + g \cos \theta_W)\mathcal{O}_{1i} - g_H\mathcal{O}_{2i} - 2g_X\mathcal{O}_{3i}] , \quad (\text{A15})$$

$$\tilde{C}_{i2} = \frac{1}{2}v_\Phi (g_H\mathcal{O}_{2i} - g_X\mathcal{O}_{3i}) , \quad (\text{A16})$$

$$\tilde{C}_{i3} = M_X\mathcal{O}_{3i} . \quad (\text{A17})$$

To cancel the mixing term in the last expression in Eq. (A13), we need the following gauge fixing term,

$$-\frac{1}{2\xi_i} (\partial_\mu Z_i^\mu - \xi_i G_i)^2 , \quad (\text{A18})$$

where ξ_i are three arbitrary gauge parameters. This gauge fixing term will not only modify the propagator of Z_i but also induce a 3×3 mass mixing matrix \mathcal{M}_G^2 among the three fields $\{G^0, G_H^0, \mathcal{S}\}$ to be ξ_i -dependence, namely

$$\mathcal{M}_G^2 = \begin{pmatrix} \mathcal{M}_{11}^2 & \mathcal{M}_{12}^2 & \mathcal{M}_{13}^2 \\ \mathcal{M}_{21}^2 & \mathcal{M}_{22}^2 & \mathcal{M}_{23}^2 \\ \mathcal{M}_{31}^2 & \mathcal{M}_{32}^2 & \mathcal{M}_{33}^2 \end{pmatrix} , \quad (\text{A19})$$

with the following matrix elements

$$\begin{aligned} \mathcal{M}_{11}^2 &= \xi_1 \tilde{C}_{11}^2 + \xi_2 \tilde{C}_{21}^2 + \xi_3 \tilde{C}_{31}^2 , \\ \mathcal{M}_{12}^2 &= \xi_1 \tilde{C}_{11} \tilde{C}_{12} + \xi_2 \tilde{C}_{21} \tilde{C}_{22} + \xi_3 \tilde{C}_{31} \tilde{C}_{32} = \mathcal{M}_{21}^2 , \\ \mathcal{M}_{13}^2 &= \xi_1 \tilde{C}_{11} \tilde{C}_{13} + \xi_2 \tilde{C}_{21} \tilde{C}_{23} + \xi_3 \tilde{C}_{31} \tilde{C}_{33} = \mathcal{M}_{31}^2 , \\ \mathcal{M}_{22}^2 &= \xi_1 \tilde{C}_{12}^2 + \xi_2 \tilde{C}_{22}^2 + \xi_3 \tilde{C}_{32}^2 , \\ \mathcal{M}_{23}^2 &= \xi_1 \tilde{C}_{12} \tilde{C}_{13} + \xi_2 \tilde{C}_{22} \tilde{C}_{23} + \xi_3 \tilde{C}_{32} \tilde{C}_{33} = \mathcal{M}_{32}^2 , \\ \mathcal{M}_{33}^2 &= \xi_1 \tilde{C}_{13}^2 + \xi_2 \tilde{C}_{23}^2 + \xi_3 \tilde{C}_{33}^2 . \end{aligned} \quad (\text{A20})$$

While the eigenvalues of \mathcal{M}_G^2 are complicated functions of the gauge fixing parameters, its determinant takes a simple form,

$$\begin{aligned} \text{Det} \mathcal{M}_G^2 &= \xi_1 \xi_2 \xi_3 \left(\tilde{C}_{11} \tilde{C}_{23} \tilde{C}_{32} + \tilde{C}_{12} \tilde{C}_{21} \tilde{C}_{33} + \tilde{C}_{13} \tilde{C}_{22} \tilde{C}_{31} \right. \\ &\quad \left. - \tilde{C}_{13} \tilde{C}_{21} \tilde{C}_{32} - \tilde{C}_{11} \tilde{C}_{22} \tilde{C}_{33} - \tilde{C}_{12} \tilde{C}_{23} \tilde{C}_{31} \right)^2 . \end{aligned} \quad (\text{A21})$$

Thus as any one of the gauge fixing parameters $\xi_i \rightarrow 0$, the corresponding Goldstone boson G_i has vanishing mass, reproducing the result of 't Hooft-Landau gauge.

This completes our discussions of all the gauge fixing terms in G2HDM. With these gauge fixing terms at hand, one can straightforwardly obtain the gauge fixing functions and

the procedure of Faddeev-Popov quantization can be proceeded as usual. Of course physical observables if computed correctly should be independent of all the otherwise arbitrary gauge fixing parameters ξ s discussed in this Appendix! In an ideal world, one would compute things using arbitrary ξ s and show the dependence of ξ s is completely dropped out at the end for any physical observable. In practice, things are hardly get done that way.

-
- [1] V. Silveira and A. Zee, “Scalar Phantoms,” *Phys. Lett. B* **161**, 136-140 (1985)
- [2] N. G. Deshpande and E. Ma, “Pattern of Symmetry Breaking with Two Higgs Doublets,” *Phys. Rev. D* **18**, 2574 (1978)
- [3] E. Ma, “Verifiable radiative seesaw mechanism of neutrino mass and dark matter,” *Phys. Rev. D* **73**, 077301 (2006) [arXiv:hep-ph/0601225 [hep-ph]].
- [4] A. H. Chamseddine, R. L. Arnowitt and P. Nath, “Locally Supersymmetric Grand Unification,” *Phys. Rev. Lett.* **49**, 970 (1982)
- [5] P. Nath, R. L. Arnowitt and A. H. Chamseddine, “Gravity Induced Symmetry Breaking and Ground State of Local Supersymmetric {GUTs},” *Phys. Lett. B* **121**, 33-36 (1983)
- [6] H. P. Nilles, “Supersymmetry, Supergravity and Particle Physics,” *Phys. Rept.* **110**, 1-162 (1984)
- [7] H. C. Cheng and I. Low, “TeV symmetry and the little hierarchy problem,” *JHEP* **09**, 051 (2003) [arXiv:hep-ph/0308199 [hep-ph]].
- [8] H. C. Cheng and I. Low, “Little hierarchy, little Higgses, and a little symmetry,” *JHEP* **08**, 061 (2004) [arXiv:hep-ph/0405243 [hep-ph]].
- [9] I. Low, “T parity and the littlest Higgs,” *JHEP* **10**, 067 (2004) [arXiv:hep-ph/0409025 [hep-ph]].
- [10] J. McDonald, “Gauge singlet scalars as cold dark matter,” *Phys. Rev. D* **50**, 3637-3649 (1994) [arXiv:hep-ph/0702143 [hep-ph]].
- [11] C. P. Burgess, M. Pospelov and T. ter Veldhuis, “The Minimal model of nonbaryonic dark matter: A Singlet scalar,” *Nucl. Phys. B* **619**, 709-728 (2001) [arXiv:hep-ph/0011335 [hep-ph]].
- [12] K. Cheung, Y. L. S. Tsai, P. Y. Tseng, T. C. Yuan and A. Zee, “Global Study of the Simplest Scalar Phantom Dark Matter Model,” *JCAP* **10**, 042 (2012) [arXiv:1207.4930 [hep-ph]].
- [13] R. Barbieri, L. J. Hall and V. S. Rychkov, “Improved naturalness with a heavy Higgs: An Alternative road to LHC physics,” *Phys. Rev. D* **74**, 015007 (2006) [arXiv:hep-ph/0603188 [hep-ph]].
- [14] L. Lopez Honorez, E. Nezri, J. F. Oliver and M. H. G. Tytgat, “The Inert Doublet Model: An Archetype for Dark Matter,” *JCAP* **02**, 028 (2007) [arXiv:hep-ph/0612275 [hep-ph]].

- [15] A. Arhrib, Y. L. S. Tsai, Q. Yuan and T. C. Yuan, “An Updated Analysis of Inert Higgs Doublet Model in light of the Recent Results from LUX, PLANCK, AMS-02 and LHC,” *JCAP* **06**, 030 (2014) [arXiv:1310.0358 [hep-ph]].
- [16] A. Belyaev, G. Cacciapaglia, I. P. Ivanov, F. Rojas-Abatte and M. Thomas, “Anatomy of the Inert Two Higgs Doublet Model in the light of the LHC and non-LHC Dark Matter Searches,” *Phys. Rev. D* **97**, no.3, 035011 (2018) [arXiv:1612.00511 [hep-ph]].
- [17] Y. L. S. Tsai, V. Tran and C. T. Lu, “Confronting dark matter co-annihilation of Inert two Higgs Doublet Model with a compressed mass spectrum,” *JHEP* **06**, 033 (2020) [arXiv:1912.08875 [hep-ph]].
- [18] S. Fabian, F. Goertz and Y. Jiang, “Dark Matter and Nature of Electroweak Phase Transition with an Inert Doublet,” [arXiv:2012.12847 [hep-ph]].
- [19] S. Akula, B. Altunkaynak, D. Feldman, P. Nath and G. Peim, “Higgs Boson Mass Predictions in SUGRA Unification, Recent LHC-7 Results, and Dark Matter,” *Phys. Rev. D* **85**, 075001 (2012) [arXiv:1112.3645 [hep-ph]].
- [20] R. L. Arnowitt and P. Nath, “Predictions of neutralino dark matter event rates in minimal supergravity unification,” *Phys. Rev. D* **54**, 2374-2384 (1996) [arXiv:hep-ph/9509260 [hep-ph]].
- [21] G. Jungman, M. Kamionkowski and K. Griest, “Supersymmetric dark matter,” *Phys. Rept.* **267**, 195-373 (1996) [arXiv:hep-ph/9506380 [hep-ph]].
- [22] C. S. Chen, K. Cheung and T. C. Yuan, “Novel Collider Signature for Little Higgs Dark Matter Models,” *Phys. Lett. B* **644**, 158-164 (2007) [arXiv:hep-ph/0605314 [hep-ph]].
- [23] C. D. Carone and R. Ramos, “Classical scale-invariance, the electroweak scale and vector dark matter,” *Phys. Rev. D* **88**, 055020 (2013) [arXiv:1307.8428 [hep-ph]].
- [24] H. Davoudiasl and I. M. Lewis, “Dark Matter from Hidden Forces,” *Phys. Rev. D* **89**, no.5, 055026 (2014) [arXiv:1309.6640 [hep-ph]].
- [25] B. Barman, S. Bhattacharya, S. K. Patra and J. Chakraborty, “Non-Abelian Vector Boson Dark Matter, its Unified Route and signatures at the LHC,” *JCAP* **12**, 021 (2017) [arXiv:1704.04945 [hep-ph]].
- [26] B. Barman, S. Bhattacharya and M. Zakeri, “Non-Abelian Vector Boson as FIMP Dark Matter,” *JCAP* **02**, 029 (2020) [arXiv:1905.07236 [hep-ph]].
- [27] T. Abe, M. Fujiwara, J. Hisano and K. Matsushita, “A model of electroweakly interacting

- non-abelian vector dark matter,” *JHEP* **07**, 136 (2020) [arXiv:2004.00884 [hep-ph]].
- [28] Z. Hu, C. Cai, Y. L. Tang, Z. H. Yu and H. H. Zhang, *JHEP* **07**, 089 (2021) [arXiv:2103.00220 [hep-ph]].
- [29] Q. H. Cao, C. R. Chen, C. S. Li and H. Zhang, “Effective Dark Matter Model: Relic density, CDMS II, Fermi LAT and LHC,” *JHEP* **08**, 018 (2011) [arXiv:0912.4511 [hep-ph]].
- [30] J. Goodman, M. Ibe, A. Rajaraman, W. Shepherd, T. M. P. Tait and H. B. Yu, “Constraints on Dark Matter from Colliders,” *Phys. Rev. D* **82**, 116010 (2010) [arXiv:1008.1783 [hep-ph]].
- [31] K. Cheung, P. Y. Tseng, Y. L. S. Tsai and T. C. Yuan, “Global Constraints on Effective Dark Matter Interactions: Relic Density, Direct Detection, Indirect Detection, and Collider,” *JCAP* **05**, 001 (2012) [arXiv:1201.3402 [hep-ph]].
- [32] J. Goodman, M. Ibe, A. Rajaraman, W. Shepherd, T. M. P. Tait and H. B. Yu, “Constraints on Light Majorana dark Matter from Colliders,” *Phys. Lett. B* **695**, 185-188 (2011) [arXiv:1005.1286 [hep-ph]].
- [33] J. Goodman, M. Ibe, A. Rajaraman, W. Shepherd, T. M. P. Tait and H. B. Yu, “Gamma Ray Line Constraints on Effective Theories of Dark Matter,” *Nucl. Phys. B* **844**, 55-68 (2011) [arXiv:1009.0008 [hep-ph]].
- [34] K. Cheung, P. Y. Tseng and T. C. Yuan, “Cosmic Antiproton Constraints on Effective Interactions of the Dark Matter,” *JCAP* **01**, 004 (2011) [arXiv:1011.2310 [hep-ph]].
- [35] K. Cheung, P. Y. Tseng and T. C. Yuan, “Gamma-ray Constraints on Effective Interactions of the Dark Matter,” *JCAP* **06**, 023 (2011) [arXiv:1104.5329 [hep-ph]].
- [36] W. C. Huang, K. W. Ng and T. C. Yuan, “Circularly Polarized Gamma Rays in Effective Dark Matter Theory,” *Phys. Lett. B* **800**, 135104 (2020) [arXiv:1907.02402 [hep-ph]].
- [37] T. Nath Maity and F. S. Queiroz, [arXiv:2104.02700 [hep-ph]].
- [38] W. C. Huang, Y. L. S. Tsai and T. C. Yuan, “G2HDM : Gauged Two Higgs Doublet Model,” *JHEP* **1604**, 019 (2016) [arXiv:1512.00229 [hep-ph]].
- [39] C. R. Chen, Y. X. Lin, C. S. Nugroho, R. Ramos, Y. L. S. Tsai and T. C. Yuan, “Complex scalar dark matter in the gauged two-Higgs-doublet model,” *Phys. Rev. D* **101**, no.3, 035037 (2020) [arXiv:1910.13138 [hep-ph]].
- [40] R. N. Mohapatra and G. Senjanovic, “Neutrino Mass and Spontaneous Parity Nonconservation,” *Phys. Rev. Lett.* **44**, 912 (1980)
- [41] R. N. Mohapatra and G. Senjanovic, “Neutrino Masses and Mixings in Gauge Models with

- Spontaneous Parity Violation,” *Phys. Rev. D* **23**, 165 (1981)
- [42] For a general review of 2HDM, see for example G. C. Branco, P. M. Ferreira, L. Lavoura, M. N. Rebelo, M. Sher and J. P. Silva, “Theory and phenomenology of two-Higgs-doublet models,” *Phys. Rept.* **516**, 1-102 (2012) [arXiv:1106.0034 [hep-ph]].
- [43] A. Arhrib, W. C. Huang, R. Ramos, Y. L. S. Tsai and T. C. Yuan, “Consistency of a gauged two-Higgs-doublet model: Scalar sector,” *Phys. Rev. D* **98**, no.9, 095006 (2018) [arXiv:1806.05632 [hep-ph]].
- [44] C. T. Huang, R. Ramos, V. Q. Tran, Y. L. S. Tsai and T. C. Yuan, “Consistency of Gauged Two Higgs Doublet Model: Gauge Sector,” *JHEP* **1909** (2019) 048 [arXiv:1905.02396 [hep-ph]].
- [45] G. ’t Hooft, “Magnetic Monopoles in Unified Gauge Theories,” *Nucl. Phys. B* **79**, 276-284 (1974)
- [46] A. M. Polyakov, “Particle Spectrum in the Quantum Field Theory,” *JETP Lett.* **20**, 194-195 (1974) PRINT-74-1566 (LANDAU-INST).
- [47] B. Julia and A. Zee, “Poles with Both Magnetic and Electric Charges in Nonabelian Gauge Theory,” *Phys. Rev. D* **11**, 2227-2232 (1975)
- [48] S. Baek, P. Ko and W. I. Park, “Hidden sector monopole, vector dark matter and dark radiation with Higgs portal,” *JCAP* **10**, 067 (2014) [arXiv:1311.1035 [hep-ph]].
- [49] N. Aghanim *et al.* [Planck], “Planck 2018 results. VI. Cosmological parameters,” *Astron. Astrophys.* **641**, A6 (2020) [arXiv:1807.06209 [astro-ph.CO]].
- [50] G. Angloher *et al.* [CRESST], “Results on MeV-scale dark matter from a gram-scale cryogenic calorimeter operated above ground,” *Eur. Phys. J. C* **77**, no.9, 637 (2017) [arXiv:1707.06749 [astro-ph.CO]].
- [51] P. Agnes *et al.* [DarkSide], “Low-Mass Dark Matter Search with the DarkSide-50 Experiment,” *Phys. Rev. Lett.* **121**, no.8, 081307 (2018) [arXiv:1802.06994 [astro-ph.HE]].
- [52] E. Aprile *et al.* [XENON], “Light Dark Matter Search with Ionization Signals in XENON1T,” *Phys. Rev. Lett.* **123**, no.25, 251801 (2019) [arXiv:1907.11485 [hep-ex]].
- [53] M. Ackermann *et al.* [Fermi-LAT], “Searching for Dark Matter Annihilation from Milky Way Dwarf Spheroidal Galaxies with Six Years of Fermi Large Area Telescope Data,” *Phys. Rev. Lett.* **115**, no.23, 231301 (2015) [arXiv:1503.02641 [astro-ph.HE]].
- [54] A. Albert *et al.* [Fermi-LAT and DES], “Searching for Dark Matter Annihilation in Re-

- cently Discovered Milky Way Satellites with Fermi-LAT,” *Astrophys. J.* **834**, no.2, 110 (2017) [arXiv:1611.03184 [astro-ph.HE]].
- [55] M. Aaboud *et al.* [ATLAS], “Search for dark matter and other new phenomena in events with an energetic jet and large missing transverse momentum using the ATLAS detector,” *JHEP* **01**, 126 (2018) [arXiv:1711.03301 [hep-ex]].
- [56] [ATLAS], “Search for new phenomena in events with jets and missing transverse momentum in p p collisions at $\sqrt{s} = 13$ TeV with the ATLAS detector,” ATLAS-CONF-2020-048.
- [57] A. M. Sirunyan *et al.* [CMS], “Search for dark matter produced with an energetic jet or a hadronically decaying W or Z boson at $\sqrt{s} = 13$ TeV,” *JHEP* **07**, 014 (2017) [arXiv:1703.01651 [hep-ex]].
- [58] R. Ramos, Van Que Tran and T. C. Yuan, *Phys. Rev. D* **103**, no.7, 075021 (2021) [arXiv:2101.07115 [hep-ph]].
- [59] P. A. Zyla *et al.* [Particle Data Group], “Review of Particle Physics,” *PTEP* **2020**, no.8, 083C01 (2020).
- [60] B. Dirgantara and C. S. Nugroho, “Effects of New Heavy Fermions on Complex Scalar Dark Matter Phenomenology in Gauged Two Higgs Doublet Model,” [arXiv:2012.13170 [hep-ph]].
- [61] D. Feldman, Z. Liu and P. Nath, “Probing a very narrow Z-prime boson with CDF and D0 data,” *Phys. Rev. Lett.* **97**, 021801 (2006) [hep-ph/0603039].
- [62] M. Fabbrichesi, E. Gabrielli and G. Lanfranchi, “The Dark Photon,” [arXiv:2005.01515 [hep-ph]].
- [63] R. Aaij *et al.* [LHCb], “Search for $A' \rightarrow \mu^+ \mu^-$ Decays,” *Phys. Rev. Lett.* **124**, no.4, 041801 (2020) [arXiv:1910.06926 [hep-ex]].
- [64] J. P. Lees *et al.* [BaBar], “Search for a Dark Photon in e^+e^- Collisions at BaBar,” *Phys. Rev. Lett.* **113**, no.20, 201801 (2014) [arXiv:1406.2980 [hep-ex]].
- [65] J. R. Batley *et al.* [NA48/2], “Search for the dark photon in π^0 decays,” *Phys. Lett. B* **746**, 178-185 (2015) [arXiv:1504.00607 [hep-ex]].
- [66] D. Banerjee *et al.* [NA64], “Search for a Hypothetical 16.7 MeV Gauge Boson and Dark Photons in the NA64 Experiment at CERN,” *Phys. Rev. Lett.* **120**, no.23, 231802 (2018) [arXiv:1803.07748 [hep-ex]].
- [67] E. M. Riordan, M. W. Krasny, K. Lang, P. De Barbaro, A. Bodek, S. Dasu, N. Varelas, X. Wang, R. G. Arnold and D. Benton, *et al.* “A Search for Short Lived Axions in an Electron

- Beam Dump Experiment,” Phys. Rev. Lett. **59**, 755 (1987)
- [68] J. Blümlein and J. Brunner, “New Exclusion Limits for Dark Gauge Forces from Beam-Dump Data,” Phys. Lett. B **701**, 155-159 (2011) [arXiv:1104.2747 [hep-ex]].
- [69] J. Blümlein and J. Brunner, “New Exclusion Limits on Dark Gauge Forces from Proton Bremsstrahlung in Beam-Dump Data,” Phys. Lett. B **731**, 320-326 (2014) [arXiv:1311.3870 [hep-ph]].
- [70] J. B. Dent, F. Ferrer and L. M. Krauss, “Constraints on Light Hidden Sector Gauge Bosons from Supernova Cooling,” [arXiv:1201.2683 [astro-ph.CO]];
- S. N. Gninenko, “Constraints on sub-GeV hidden sector gauge bosons from a search for heavy neutrino decays,” Phys. Lett. B **713**, 244-248 (2012) [arXiv:1204.3583 [hep-ph]];
- H. K. Dreiner, J. F. Fortin, C. Hanhart and L. Ubaldi, “Supernova constraints on MeV dark sectors from e^+e^- annihilations,” Phys. Rev. D **89**, no.10, 105015 (2014) [arXiv:1310.3826 [hep-ph]];
- H. Merkel *et al.*, “Search at the Mainz Microtron for Light Massive Gauge Bosons Relevant for the Muon $g-2$ Anomaly,” Phys. Rev. Lett. **112**, no.22, 221802 (2014) [arXiv:1404.5502 [hep-ex]];
- B. Batell, R. Essig and Z. Surujon, “Strong Constraints on Sub-GeV Dark Sectors from SLAC Beam Dump E137,” Phys. Rev. Lett. **113**, no.17, 171802 (2014) [arXiv:1406.2698 [hep-ph]];
- A. Anastasi *et al.* [KLOE-2], “Limit on the production of a new vector boson in $e^+e^- \rightarrow U\gamma$, $U \rightarrow \pi^+\pi^-$ with the KLOE experiment,” Phys. Lett. B **757**, 356-361 (2016) [arXiv:1603.06086 [hep-ex]];
- L. Marsicano, M. Battaglieri, M. Bondí, C. D. R. Carvajal, A. Celentano, M. De Napoli, R. De Vita, E. Nardi, M. Raggi and P. Valente, “Dark photon production through positron annihilation in beam-dump experiments,” Phys. Rev. D **98**, no.1, 015031 (2018) [arXiv:1802.03794 [hep-ex]];
- CMS Collaboration, “Search for a narrow resonance decaying to a pair of muons in proton-proton collisions at 13 TeV,” CMS-PAS-EXO-19-018.
- [71] G. Aad *et al.* [ATLAS], “Combined measurements of Higgs boson production and decay using up to 80 fb^{-1} of proton-proton collision data at $\sqrt{s} = 13 \text{ TeV}$ collected with the ATLAS experiment,” Phys. Rev. D **101**, no.1, 012002 (2020) [arXiv:1909.02845 [hep-ex]].
- [72] A. M. Sirunyan *et al.* [CMS], “Combined measurements of Higgs boson couplings in proton-

- proton collisions at $\sqrt{s} = 13 \text{ TeV}$,” *Eur. Phys. J. C* **79**, no.5, 421 (2019) [arXiv:1809.10733 [hep-ex]].
- [73] [ATLAS], “Search for invisible Higgs boson decays with vector boson fusion signatures with the ATLAS detector using an integrated luminosity of 139 fb^{-1} ,” ATLAS-CONF-2020-008.
- [74] G. Arcadi, M. Dutra, P. Ghosh, M. Lindner, Y. Mambrini, M. Pierre, S. Profumo and F. S. Queiroz, “The waning of the WIMP? A review of models, searches, and constraints,” *Eur. Phys. J. C* **78**, no.3, 203 (2018) [arXiv:1703.07364 [hep-ph]].
- [75] M. Escudero, A. Berlin, D. Hooper and M. X. Lin, “Toward (Finally!) Ruling Out Z and Higgs Mediated Dark Matter Models,” *JCAP* **12**, 029 (2016) [arXiv:1609.09079 [hep-ph]].
- [76] J. L. Feng, J. Kumar, D. Marfatia and D. Sanford, “Isospin-Violating Dark Matter,” *Phys. Lett. B* **703**, 124-127 (2011) [arXiv:1102.4331 [hep-ph]].
- [77] C. E. Yaguna, “Isospin-violating dark matter in the light of recent data,” *Phys. Rev. D* **95**, no.5, 055015 (2017) [arXiv:1610.08683 [hep-ph]].
- [78] J. Alwall, M. Herquet, F. Maltoni, O. Mattelaer and T. Stelzer, “MadGraph 5 : Going Beyond,” *JHEP* **06**, 128 (2011) [arXiv:1106.0522 [hep-ph]].
- [79] B. Dumont, B. Fuks, S. Kraml, S. Bein, G. Chalons, E. Conte, S. Kulkarni, D. Sengupta and C. Wymant, “Toward a public analysis database for LHC new physics searches using MadAnalysis 5,” *Eur. Phys. J. C* **75**, no.2, 56 (2015) [arXiv:1407.3278 [hep-ph]].
- [80] G. Apollinari, O. Brüning, T. Nakamoto and L. Rossi, “High Luminosity Large Hadron Collider HL-LHC,” CERN Yellow Rep., no.5, 1-19 (2015) [arXiv:1705.08830 [physics.acc-ph]].
- [81] M. Benedikt and F. Zimmermann, “Proton Colliders at the Energy Frontier,” *Nucl. Instrum. Meth. A* **907**, 200-208 (2018) [arXiv:1803.09723 [physics.acc-ph]].
- [82] N. Arkani-Hamed, T. Han, M. Mangano and L. T. Wang, “Physics opportunities of a 100 TeV proton–proton collider,” *Phys. Rept.* **652**, 1-49 (2016) [arXiv:1511.06495 [hep-ph]].
- [83] G. Bélanger, F. Boudjema, A. Goudelis, A. Pukhov and B. Zaldivar, “micrOMEGAs5.0 : Freeze-in,” *Comput. Phys. Commun.* **231**, 173-186 (2018) [arXiv:1801.03509 [hep-ph]].
- [84] A. Alloul, N. D. Christensen, C. Degrande, C. Duhr and B. Fuks, “FeynRules 2.0 - A complete toolbox for tree-level phenomenology,” *Comput. Phys. Commun.* **185**, 2250-2300 (2014) [arXiv:1310.1921 [hep-ph]].
- [85] A. Belyaev, N. D. Christensen and A. Pukhov, “CalcHEP 3.4 for collider physics within and beyond the Standard Model,” *Comput. Phys. Commun.* **184**, 1729-1769 (2013) [arXiv:1207.6082

- [hep-ph]].
- [86] D. Foreman-Mackey, D. W. Hogg, D. Lang and J. Goodman, “emcee: The MCMC Hammer,” *Publ. Astron. Soc. Pac.* **125**, 306-312 (2013) [arXiv:1202.3665 [astro-ph.IM]].
- [87] M. Battaglieri, A. Belloni, A. Chou, P. Cushman, B. Echenard, R. Essig, J. Estrada, J. L. Feng, B. Flaugher and P. J. Fox, *et al.* “US Cosmic Visions: New Ideas in Dark Matter 2017: Community Report,” [arXiv:1707.04591 [hep-ph]].
- [88] R. Agnese *et al.* [SuperCDMS], “Projected Sensitivity of the SuperCDMS SNOLAB experiment,” *Phys. Rev. D* **95**, no.8, 082002 (2017) [arXiv:1610.00006 [physics.ins-det]].
- [89] H. Ma *et al.* [CDEX], “CDEX Dark Matter Experiment: Status and Prospects,” *J. Phys. Conf. Ser.* **1342**, no.1, 012067 (2020) [arXiv:1712.06046 [hep-ex]].
- [90] E. Kou *et al.* [Belle-II], “The Belle II Physics Book,” *PTEP* **2019**, no.12, 123C01 (2019) [erratum: *PTEP* **2020**, no.2, 029201 (2020)] [arXiv:1808.10567 [hep-ex]].
- [91] D. Banerjee *et al.*, “Addendum to the NA64 Proposal: search for $A' \rightarrow$ invisible and $X \rightarrow e^+e^-$ decays in 2021,” CERN-SPSC-2018-004 (SPSC-P-348-ADD-2).
- [92] A. Caldwell, J. Chappell, P. Crivelli, E. Depero, J. Gall, S. Gninenko, E. Gschwendtner, A. Hartin, F. Keeble and J. Osborne, *et al.* “Particle physics applications of the AWAKE acceleration scheme,” [arXiv:1812.11164 [physics.acc-ph]].
- [93] M. D’Onofrio, O. Fischer and Z. S. Wang, “Searching for Dark Photons at the LHeC and FCC-he,” *Phys. Rev. D* **101**, no.1, 015020 (2020) [arXiv:1909.02312 [hep-ph]].